

Neoproterozoic anatexis of Archean lithosphere: Geochemical evidence from felsic to mafic intrusions at Xiaofeng in the Yangtze Gorge, South China

Shao-Bing Zhang^{a,b,*}, Yong-Fei Zheng^{a,c,*}, Zi-Fu Zhao^a, Yuan-Bao Wu^d, Honglin Yuan^c, Fu-Yuan Wu^b

^a CAS Key Laboratory of Crust-Mantle Materials and Environments, School of Earth and Space Sciences, University of Science and Technology of China, Hefei 230026, China

^b State Key Laboratory of Lithospheric Evolution, Institute of Geology and Geophysics, Chinese Academy of Sciences, Beijing 100029, China

^c State Key Laboratory of Continental Dynamics, Department of Geology, Northwest University, Xi'an 710069, China

^d State Key Laboratory of Geological Processes and Mineral Resources, Faculty of Earth Sciences, China University of Geosciences, Wuhan 430074, China

Received 19 June 2007; received in revised form 12 October 2007; accepted 22 December 2007

Abstract

An integrated study of geochronology and geochemistry was carried out for Neoproterozoic intrusions at Xiaofeng in the Yangtze Gorge. The results are used to provide constraints on their origin, with potential resolution to hotly debated models concerning the source and process of contemporaneous igneous rocks in South China. The Xiaofeng intrusions are composed of felsic–mafic dykes and their wall-rock granitoids in an area of <10 km². They show intrusion relationship to TTG rocks of the Archean Kongling Complex. Zircon U–Pb dating indicates that the dykes and granitoids were crystallized almost contemporaneously at 800 ± 3 Ma. They share similar distribution patterns of REE and trace elements, i.e. enrichment in LILE and LREE but depletion in HFSE. The dykes have whole-rock $\epsilon_{Nd}(t)$ values of –9.9 to –6.4 and zircon $\epsilon_{Hf}(t)$ values of about –12.9 to –9.0, and the granitoids have whole-rock $\epsilon_{Nd}(t)$ values of –10.6 to –9.2 and zircon $\epsilon_{Hf}(t)$ values of –10.5 to –8.3. Furthermore, their zircon Hf model ages are similar to each other, from 2.8 to 3.2 Ga. These results indicate that they both are derived from reworking of Mesoproterozoic lithosphere, with the difference only in major element composition. Zircon has $\delta^{18}O$ values of 5.4–6.8‰ for them, typical for I-type granite. Mineral O isotopes indicate small-scale high-T water–rock interaction during the intrusion of the dykes into the granitoids. No growth of juvenile crust during the middle Neoproterozoic magmatism is identified to occur in the Xiaofeng intrusions. Thus, neither mantle plume nor oceanic arc is responsible for their origin, ruling out the plume–rift and slab–arc models for their petrogenesis. Instead, the Neoproterozoic anatexis of the Archean lithosphere can be explained by the tectonic collapse of a thickened intracontinental orogen that formed by Paleoproterozoic arc–continent collision to the Archean Kongling Complex, but it became molten due to lithospheric extension in response to plate reorganization prior to breakup of the supercontinent Rodinia. This provides a positive test to the plate–rift model for their petrogenesis.

© 2008 Elsevier B.V. All rights reserved.

Keywords: Zircon; U–Pb age; Hf isotope; O isotope; Neoproterozoic magmatism; Orogenic collapse

1. Introduction

One of the most significant characteristics of South China is the widespread occurrence of Neoproterozoic igneous rocks, mainly granitoids and mafic rocks in ages from 830 to 740 Ma, along the periphery of the Yangtze Block (e.g., Li et al., 2003a; Zheng et al., 2004). With respect to their petrogenesis, however, there has been much controversy in the last few years (e.g., Wang et al., 2004a,b; Li et al., 2004a, 2007a,b; Zhou et al., 2007;

* Corresponding authors at: CAS Key Laboratory of Crust-Mantle Materials and Environments, School of Earth and Space Sciences, University of Science and Technology of China, Hefei 230026, China. Tel.: +86 5513603554; fax: +86 5513603554.

E-mail addresses: sbzhang@ustc.edu.cn (S.-B. Zhang), yfzheng@ustc.edu.cn (Y.-F. Zheng).

Munteanu and Yao, 2007). Generally, three types of model have been suggested. (1) Plume-rift model, envisaging a mantle plume at about 825 Ma (Li et al., 1999, 2002a), then a mantle super-plume event at 830–740 Ma (Li et al., 2003a,b), to cause the Rodinia breakup and rift magmatism in South China. However, the existence of mantle plumes at that time has become a subject of hot debates. (2) Island-arc model, supposing formation of the Neoproterozoic igneous rocks along active continental margins by the contemporaneous subduction of oceanic crust (Zhou et al., 2002a,b). Nevertheless, it remains to be tested whether the arc magmatic rocks have the origin of juvenile crust with linear occurrences. (3) Plate-rift model, assuming the Neoproterozoic magmatism resulting from lithospheric extension in response to the tectonic evolution from supercontinental rift to breakup (Zheng et al., 2007). Reworking of both juvenile and ancient crusts is suggested due to either tectonic collapse of, or rifting melting along, preexisting arc-continent collision orogens. To test which model is reasonable appeals a resolution to paradoxical interpretations concerning trace element and isotope patterns of both arc-like and rift-like sources in given igneous suites.

So far intensive studies of geochronology and geochemistry were principally focused on igneous rocks at the margin of the Yangtze Block (Fig. 1a), including the Jiangnan Orogen along its southeastern margin (Li et al., 1999, 2002b, 2003b; Wang et al., 2004b, 2006; Zhou et al., 2004; Wu et al., 2006a; Zheng et al., 2007), the Kangdian Rift along its western margin (Li et al., 2002a,b, 2003a, 2005, 2006; Zhou et al., 2002a,b, 2006a,b; Zhao and Zhou, 2006; Lin et al., 2007; Zheng et al., 2007), and the Dabie-Sulu Orogen along its northern margin (Ames et al., 1996; Hacker et al., 2000; Chen et al., 2003; Wu et al., 2004; Zheng et al., 2004, 2006a; Huang et al., 2006). Studies of the Neoproterozoic rocks in the interior of the Yangtze Block, such as the Huangling Batholith, were relatively limited (e.g., Li et al., 2003b, 2004b; Ling et al., 2006). The Xiaofeng Suite in the Huangling Batholith is particularly important because a lot of mafic dykes occur in this suite and were regarded as evidence for mantle plume (Li et al., 2004b). Thus, a combined study of zircon U–Pb age and Hf–O isotopes as well as whole-rock elements and isotopes may provide insight into the debates concerning the origin of Neoproterozoic igneous rocks in South China. For this pur-

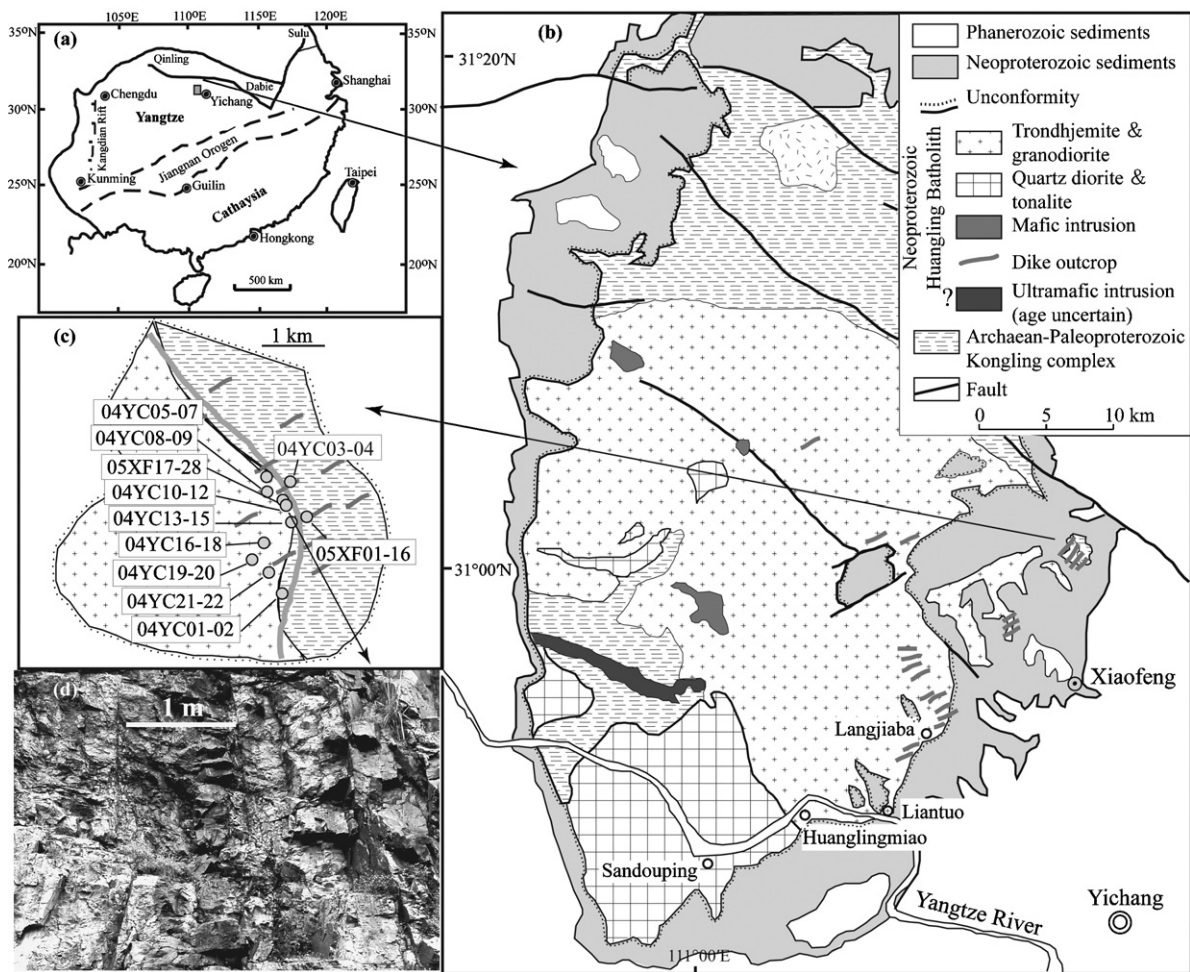


Fig. 1. Simplified geological map of the studying areas at Xiaofeng in the Yangtze Gorge, Yichang City, Hubei Province, China. (a) The location of studying area in South China. (b) Sketch map of the Huangling Anticline mainly consist of the Huangling Batholith and the Kongling Complex. (c) Detailed sample locations along the Xiaofeng River at Qilixia, Xiaofeng Town. (d) Field photos showing the relationship between mafic dykes (dark colored) and wall-rock granitoids (light colored) of the Xiaofeng Suite.

pose, we have made a detailed study of geochronology and geochemistry for the mafic dykes and their wall-rock granitoids in this area. The results place important constraints on their origin, with a geochemical test to the three types of petrogenetic model.

2. Geologic background

The Xiaofeng Suite, a part of the Huangling granitoid batholith (Fig. 1), is located at the northwest of Yichang in Hubei Province. It lies in the interior of the Yangtze Block, about 300 km to the south of the Qinling orogen. The exposed area of the Huangling Batholith is about 970 km². It intruded into the Archean–Paleoproterozoic Kongling Complex and separated the Kongling Complex into two parts. It is overlain unconformably by the Liantuo Formation, dated at 748 ± 12 Ma (Ma et al., 1984). The Kongling Complex, the Huangling Batholith, overlying Neoproterozoic and Phanerozoic sediments constitute an anticline together. The Huangling Batholith is disintegrated into four magmatic suites, namely the Huanglingmiao trondhjemite–granodiorite, the Sandouping (Taipingxi) quartz diorite–tonalite, the Dalaoling monzodiorite–monzogranite, and the Xiaofeng mafic–felsic composite suite. The Huanglingmiao and Sandouping Suites exposed about 90% of the area of the whole batholith.

The exposed area of the Xiaofeng Suite is the smallest, but it is of great significance because it contains a lot of mafic to felsic dykes. Our samples were collected at Qilixia, about 10 km north of Xiaofeng Town in Yichang. Generally, three types of igneous rocks can be recognized at this locality: (1) dark-colored dykes and light-colored dykes (e.g., 04YC11, 05XF23), which are normally considered to have mafic and felsic compositions, respectively; (2) middle-grained, fine-grained or porphyritic granitoid plutons (e.g., 04YC02, 04YC05, 04YC13) that are wall-rock of the dykes; (3) middle-grained granite and meta-granite that serve as the country rocks of the Xiaofeng Suite. Type 1 (hereafter dykes) and type 2 rocks (hereafter wall-rock granitoids) belong to the Xiaofeng Suite of the Neoproterozoic Huangling Batholith, whereas type 3 rocks (hereafter country-rock granites) mainly belong to the Kongling Archean Complex.

The dykes and wall-rock granitoids of the Xiaofeng Suite are only exposed in a quite limited area (less than 10 km²) relative to the Huangling Batholith. The trend of the dykes is about NE 65°. The dykes are sub-vertical or near vertical, with thicknesses between a few centimeters and several meters. The dykes and the wall-rock granitoids are regarded as being formed nearly simultaneously because they share the same orientation and spatial distribution. Li et al. (2004b) obtained a SHRIMP U–Pb age of 802 ± 10 Ma for a pale-grey-colored porphyritic felsic dyke.

We collected a series of samples at Qilixia, including all the three types of rocks. The mafic to felsic dykes were sampled from the same locality as Li et al. (2004b). Furthermore, two continuous profiles were sampled across the mafic dykes and wall-rock granitoids. The first profile is about 15 m in length, containing 16 samples. From the northeast to the southwest, the rock types are country-rock granite, through the dyke and the wall-rock granitoid, to the country-rock granite of the other side. The second profile (partly shown in Fig. 1d) is about 5 m

in length and contains 12 samples, but straddle across two dykes and two fine-grained wall-rock granitoids.

The wall-rock granitoids are usually middle-grained or fine-grained with major minerals of 30–40% K-feldspar, 30–40% plagioclase, 20–30% quartz. Hornblende may be another rock-forming mineral for a few samples. All feldspars in the wall-rock granitoids show different degrees of sericitization or kaolinization. Quartz in a few samples shows myrmekite-like structures. Accessory minerals usually include magnetite, chlorite and zircon. Minerals in the felsic dykes are ~50% plagioclase, ~40% hornblende and ~5% quartz and minor magnetite. The mafic dykes include gabbroic diorite, gabbro, diabase and diabase-porphry. The gabbroic diorite usually consist of ~30% pyroxene, ~20% hornblende and ~50% variably sericitized plagioclase. Pyroxenes in gabbro and diabase usually show different degrees of chloritization or epidotization. Diabase-porphry is usually composed of diabasic matrix and equal-granular porphyritic crystals, mainly pyroxene and plagioclase at the scale of ~1 mm. The country-rock granites are middle-grained, deformed at a few localities, with major minerals of 40–50% quartz, 20–30% plagioclase, 20–30% K-feldspar and minor minerals of magnetite and chlorite.

3. Analytical methods

Major elements were determined using a Varian Vista Pro ICP-AES at Guangzhou Institute of Geochemistry, and X-ray fluorescence (XRF) at University of Science and Technology of China in Hefei. ICP-AES analytical procedures are similar to those of Ramsey et al. (1995) and analytical precision is better than 1–2%. Trace element analyses were completed using an ELAN 6000 ICP-MS at Guangzhou Institute of Geochemistry, and an ELEMENT ICP-MS at Institute of Geology and Geophysics in Beijing. Procedures for ICP-MS trace element analysis were similar to those described by Li et al. (2003b). Analytical precision for most elements is better than 5%. XRF analytical procedures are similar to those described by Lee et al. (1997) and analytical precision of XRF is generally better than 1–5%.

Rb–Sr and Sm–Nd isotopic compositions were determined using a Micromass Isoprobe MC-ICPMS at Guangzhou Institute of Geochemistry. Analytical procedures were similar to those described by Li et al. (2003b). Measured ¹⁴³Nd/¹⁴⁴Nd ratios were normalized to ¹⁴⁶Nd/¹⁴⁴Nd = 0.7219, and measured ⁸⁷Sr/⁸⁶Sr ratios were normalized to ⁸⁶Sr/⁸⁸Sr = 0.1194. The measured ⁸⁷Sr/⁸⁶Sr ratio for NBS987 standard during this study is 0.710248. The ¹⁴³Nd/¹⁴⁴Nd ratios are adjusted relative to the La Jolla standard of 0.511860. Analytical precisions of isotope ratio measurements are given as $\pm 2\sigma$ standard errors.

Oxygen isotope analysis of mineral separates was conducted by the laser fluorination technique at University of Science and Technology of China in Hefei. O₂ was extracted from the minerals by a CO₂ laser and transferred to a Finigan Delta+ mass spectrometer for the measurement of ¹⁸O/¹⁶O and ¹⁷O/¹⁶O ratios (Zheng et al., 2002). O isotope data are reported as $\delta^{18}\text{O}$, which represents the per mil differences (‰) from the reference standard VSMOW. Reference minerals used in the laboratory are as follows: garnet UWG-2 with $\delta^{18}\text{O} = 5.8\text{‰}$ (Valley et al., 1995),

Table 1
Chemical composition of intrusive rocks at Xiaofeng in the Huangling Batholith

Wall-rock granitoids								
	04YC02	04YC05	04YC13	05XF11	05XF13	05XF20	05XF22	05XF27
SiO ₂	67.87	69.80	75.39	76.53	76.22	71.08	72.50	68.41
TiO ₂	0.52	0.43	0.00	0.17	0.16	0.05	0.16	0.28
Al ₂ O ₃	15.30	15.10	14.27	12.63	12.63	15.53	14.72	15.32
Fe ₂ O ₃	3.38	2.70	0.21	0.98	1.02	0.74	1.91	2.69
MgO	1.52	0.93	0.06	0.28	0.27	0.17	0.41	1.03
MnO	0.05	0.05	0.05	0.03	0.03	0.05	0.03	0.08
CaO	2.22	1.68	0.65	0.71	0.74	1.05	1.45	1.96
Na ₂ O	4.33	4.51	3.90	4.29	4.55	4.30	4.92	4.15
K ₂ O	3.06	3.30	5.48	3.85	3.37	5.77	3.00	4.96
P ₂ O ₅	0.15	0.11	0.02	0.03	0.03	0.10	0.06	0.14
LOI	1.30	1.17	0.22	0.46	1.02	1.11	0.70	0.97
Total	99.69	99.78	100.24	99.96	100.04	99.95	99.86	99.98
Sc	6.60	4.73	2.24	1.89	1.80	n.d.	0.61	7.29
V	52.5	36.6	4.7	7.46	7.13	8.3	19.9	27.0
Cr	20.4	10.8	10.6	4.05	4.38	4.87	7.55	17.3
Co	7.92	4.93	1.62	1.25	1.36	2.20	3.38	5.57
Ni	10.1	5.2	1.2	1.42	1.33	56.8	4.29	15.0
Cu	3.4	8.2	20.6	2.66	2.14	29.9	14.2	17.1
Ga	17.0	16.7	19.3	13.2	14.2	16.3	17.4	15.7
Ge	1.48	1.16	1.97					
Rb	66.5	86.7	130.4	91.0	85.6	149	67.7	82.0
Sr	336	227	74	100	102	300	429	351
Y	14.33	13.65	16.60	13.4	14.5	4.46	5.26	12.1
Zr	190	173	32	106	122	28.1	130	344
Nb	13.35	13.44	15.77	15.9	16.2	8.77	5.50	4.22
Cs	1.23	1.33	0.53	0.91	1.01	1.82	1.35	1.71
Ba	822	1023	692	1071	1020	873	766	1809
La	50.0	49.8	6.8	48.2	41.9	6.59	21.2	18.7
Ce	88.7	86.5	14.4	82.3	67.2	13.6	34.3	41.8
Pr	9.25	9.08	1.85	8.36	7.55	1.52	3.52	5.78
Nd	30.1	28.9	6.5	23.9	23.3	5.44	11.1	23.4
Sm	4.41	4.24	2.01	3.73	3.60	1.21	1.84	5.07
Eu	1.00	0.97	0.04	0.60	0.55	0.45	1.00	1.24
Gd	2.79	2.71	2.30	3.01	2.83	1.06	1.34	4.00
Tb	0.49	0.47	0.46	0.44	0.44	0.16	0.18	0.54
Dy	2.78	2.60	2.87	2.38	2.51	0.81	0.94	2.72
Ho	0.54	0.51	0.54	0.46	0.50	0.13	0.17	0.49
Er	1.47	1.45	1.52	1.30	1.47	0.32	0.45	1.24
Tm	0.22	0.23	0.28	0.21	0.24	0.04	0.07	0.18
Yb	1.47	1.53	1.94	1.43	1.64	0.24	0.41	1.12
Lu	0.26	0.25	0.32	0.22	0.26	0.03	0.06	0.16
Hf	5.09	4.66	1.58	3.54	4.10	3.36	3.48	9.06
Ta	0.98	1.05	1.26	1.15	1.17	1.69	0.42	0.16
Pb				21.7	20.1	15.2	15.9	13.4
Th	13.83	14.64	3.16	15.6	15.7	1.46	5.90	1.41
U	2.07	1.52	1.08	1.81	2.20	1.79	0.72	1.47
Mafic to felsic dykes								
	05XF05	05XF08	05XF17	05XF23	05XF24	04YC11	04YC20	
SiO ₂	53.77	54.82	55.26	50.92	50.44	66.05	56.81	
TiO ₂	1.26	1.55	1.21	1.50	1.50	0.61	1.33	
Al ₂ O ₃	15.68	15.18	16.00	17.08	16.90	15.72	16.55	
Fe ₂ O ₃	8.89	10.58	9.40	9.83	9.68	4.20	7.80	
MgO	5.72	4.83	5.02	5.39	5.44	1.81	4.64	
MnO	0.18	0.18	0.18	0.19	0.18	0.07	0.13	
CaO	6.79	6.53	6.06	7.15	7.48	3.37	5.56	
Na ₂ O	4.36	3.68	3.95	4.08	3.99	4.06	4.31	
K ₂ O	1.79	1.50	1.48	1.45	1.37	2.67	1.36	
P ₂ O ₅	0.54	0.30	0.48	0.44	0.45	0.19	0.35	
LOI	1.08	0.98	1.12	2.02	2.55	1.13	1.84	
Total	100.06	100.13	100.16	100.05	99.98	99.89	100.68	

Table 1 (Continued)

	Mafic to felsic dykes						
	05XF05	05XF08	05XF17	05XF23	05XF24	04YC11	04YC20
Sc	17.11	14.76	12.77	18.4	16.9	7.17	16.22
V	152	188	167	146	161	68.0	123.9
Cr	85.1	76.1	65.4	70.7	69.3	24.8	95.1
Co	24.8	28.0	34.5	30.6	29.7	9.82	25.81
Ni	55.4	43.9	59.5	43.7	42.0	14.0	59.9
Cu	25.9	30.3	34.4	11.4	26.8	6.0	22.7
Ga	17.4	18.4	20.3	18.2	17.8	17.4	18.7
Ge						1.39	1.73
Rb	37.9	64.2	69.0	80.5	72.4	74.6	53.7
Sr	697	567	638	675	713	470	482
Y	20.5	20.3	18.9	26.7	24.9	14.91	26.51
Zr	154	252	182	176	175	213	211
Nb	12.7	10.3	14.2	11.4	11.4	12.00	12.79
Cs	0.61	2.29	2.53	3.39	3.63	1.82	1.95
Ba	416	824	779	616	451	872	835
La	51.5	47.3	53.2	30.9	30.6	47.9	37.8
Ce	102	85.6	107.9	65.9	66.2	83.1	74.9
Pr	12.4	9.70	12.8	8.49	8.37	8.97	9.32
Nd	43.4	33.8	44.5	32.6	33.1	29.4	35.1
Sm	7.71	6.27	7.89	6.97	6.83	4.38	6.14
Eu	2.00	1.85	2.07	2.07	2.00	1.08	1.77
Gd	6.09	5.45	6.09	6.31	6.15	3.36	5.56
Tb	0.85	0.80	0.82	0.97	0.95	0.51	0.88
Dy	4.45	4.54	4.27	5.60	5.43	2.78	4.83
Ho	0.86	0.94	0.81	1.14	1.12	0.54	1.00
Er	2.27	2.55	2.07	2.98	2.97	1.50	2.63
Tm	0.32	0.37	0.30	0.44	0.43	0.23	0.39
Yb	2.02	2.37	1.83	2.74	2.65	1.50	2.62
Lu	0.30	0.37	0.27	0.41	0.41	0.25	0.42
Hf	4.22	6.39	4.84	4.64	4.62	5.24	5.23
Ta	0.67	0.57	0.74	0.63	0.64	0.79	0.81
Pb	8.17	16.0	29.0	8.65	7.09		
Th	5.44	6.27	6.80	3.53	3.18	11.64	7.21
U	1.07	0.99	1.79	0.83	0.74	1.82	1.28

Note: n.d., not detected because the concentration is lower than the detection limit.

zircon 91500 with $\delta^{18}\text{O} = 10.0\%$ (Zheng et al., 2004) and home-standard garnet 04BXL07 with $\delta^{18}\text{O} = 3.7\%$ (Gong et al., 2007). Reproducibility for repeated measurements of individual samples was better than $\pm 0.1\%$. Uncertainties of individual $\delta^{18}\text{O}$ analyses are reported with 1σ , and weighted average $\delta^{18}\text{O}$ values for the reference minerals are calculated at 2σ level.

Samples for U–Pb and Lu–Hf analysis were processed by conventional magnetic and density techniques to concentrate zircons. Representative zircons were selected by hand-picking under a binocular microscope. Then the zircons were cast in an epoxy mount and polished to section the crystals for analysis. Transmitted and reflected light micrographs and cathodoluminescence (CL) images were taken before U–Pb dating and Lu–Hf analysis to help select of analysis spots. SHRIMP U–Pb analysis for three samples were accomplished at Beijing SHRIMP Center using a SHRIMP II. Instrumental conditions and data acquisition were generally as described by Williams (1998). The data were treated following Compston et al. (1992), and then the ISO-PLOT program of Ludwig (2001). Common Pb was corrected using the measured ^{204}Pb , and errors are reported with 2σ errors. The other samples were dated by LA-ICPMS at Northwest University in Xi'an, using an Agilent 7500 equipped with a 193 nm

ArF excimer laser. Detailed analytical technique is described by Yuan et al. (2004). Spots diameters are 30 μm . Raw data were processed using GLITTER 4.0 software (Macquarie University). The common Pb was corrected by ComPbCorr#3.151 (Andersen, 2002). The results were also processed by the ISO-PLOT program of Ludwig (2001). Uncertainties of individual analyses are reported with 1σ ; weighted average ages are calculated at 2σ level.

Zircon Lu–Hf isotope analysis was carried out in situ using a Neptune multi-collector ICPMS, with a Geolas 193 nm laser ablation system, at the Institute of Geology and Geophysics in Beijing. Instrumental conditions and data acquisition were described by Xu et al. (2004) and Wu et al. (2006b). Typical ablation time for each analysis is about 30 s for 200 cycles of each measurement, with a 10 Hz repetition rate, and a laser power of 100 mJ/pulse. The analysis spots are usually 60 μm and sometimes 30 μm where the analyzed core or rim is small. $\varepsilon_{\text{Hf}}(t)$ values were calculated with the reference to the chondritic reservoir (CHUR) at the time of zircon crystallization. Parameters adopted in this study are as follows: $1.865 \times 10^{-11} \text{ year}^{-1}$ for the decay constant of ^{176}Lu (Scherer et al., 2001), 0.282772 and 0.0332 for the $^{176}\text{Hf}/^{177}\text{Hf}$ and $^{176}\text{Lu}/^{177}\text{Hf}$ ratios of the chon-

drite (Blichert-Toft and Albarede, 1997). Single-stage model ages (T_{DM1}) were calculated referred to the depleted mantle with a present-day $^{176}\text{Hf}/^{177}\text{Hf}$ ratio of 0.28325, similar to that of the average MORB (Nowell et al., 1998) and $^{176}\text{Lu}/^{177}\text{Hf}$ ratio of 0.0384 (Griffin et al., 2000). Two-stage model ages (T_{DM2}) are also calculated using a $^{176}\text{Lu}/^{177}\text{Hf}$ of 0.022 for average mafic rocks (Amelin et al., 2000) because TTG rocks are generally thought to be formed by partial melting of mafic rocks.

4. Results

4.1. Chemical composition

Fifteen samples, including eight wall-rock granitoids and seven dykes, were analyzed for their major and trace ele-

ments, and the results are listed in Table 1. SiO_2 contents are 68–77% for the granitoids and 50–66% for the dykes. All samples have high Na_2O contents of 3.68–4.92%. From the Harker diagram (Fig. 2), it can be seen that the granitoids and dykes almost form a continuous spectrum of SiO_2 contents with a gap at about 60%. They show a negative correlation between P_2O_5 and SiO_2 (Fig. 2), typical of I-type granites (Chappell, 1999). In addition, CaO , MgO , Fe_2O_3 , and TiO_2 are negatively correlated with SiO_2 . The granitoids are metaluminous to weakly peraluminous, but none of their A/CNK values is greater than 1.1 (Fig. 3). This is consistent with the classification that the granitoids are I-type granites. In the TAS diagram (Fig. 4), the granitoids mainly plot in the granite field, with a single sample in the field of quartz monzonite and granodiorite. In contrast, the dykes are mainly in the gabbro to

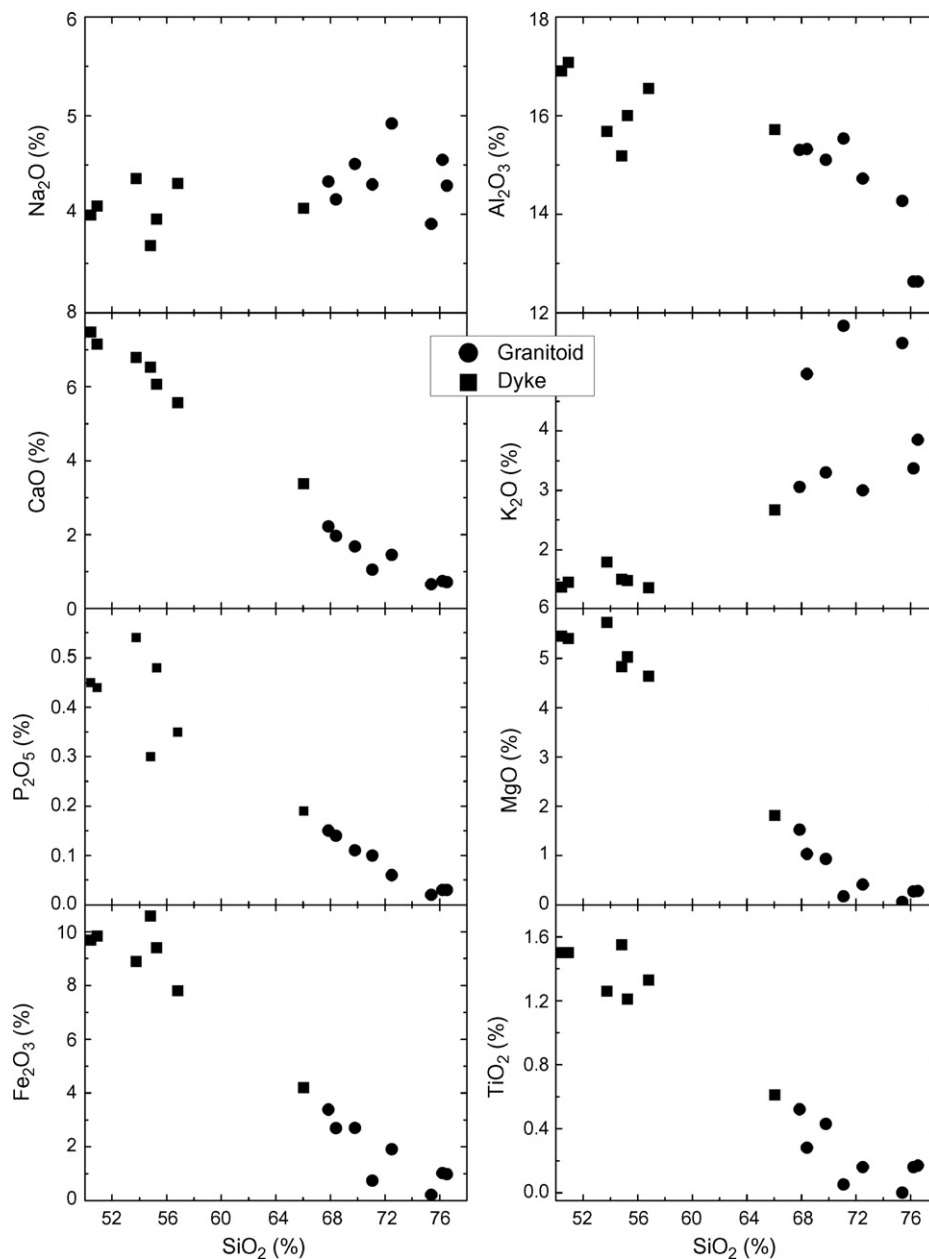


Fig. 2. The Harker diagrams for dykes and wall-rock granitoids in the Xiaofeng Suite.

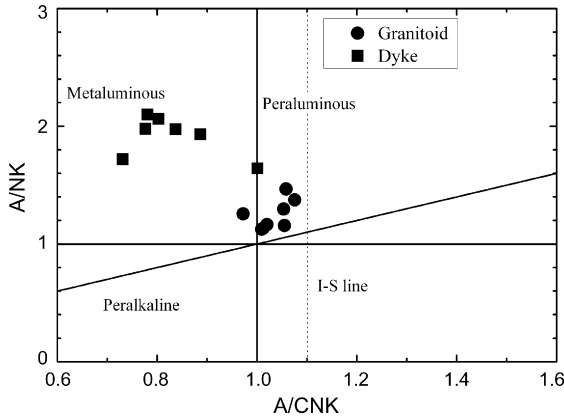


Fig. 3. Plot of A/NK ($\text{Al}_2\text{O}_3/\text{Na}_2\text{O} + \text{K}_2\text{O}$) vs. A/CNK ($\text{Al}_2\text{O}_3/\text{CaO} + \text{Na}_2\text{O} + \text{K}_2\text{O}$) for Neoproterozoic dykes and wall-rock granitoids in the Xiaofeng Suite.

gabbrodiorite field, with one having granodioritic composition.

Patterns of Ba and Zr covariation for the Xiaofeng Suite (Fig. 5) are similar to those of the Boggy Plain Pluton in the Lachlan Fold Belt, southeastern Australia (Chappell et al., 2004). Both Zr and Ba concentrations increase with increasing SiO_2 for the mafic rocks. But they decrease with increasing SiO_2 for the granitoids, forming an inflexion at the intermediate compositions. This implies that Zr was not saturated in the mafic melts, but it was saturated in the more felsic melts. Although zircons are present in the mafic dykes, they crystallized in relatively late stage because they have irregular shapes that were apparently imposed by early-formed minerals between which they crystallized. Zircon is one of the earliest crystallized minerals in felsic magma because Zr is usually saturated in the felsic melt. The variations of Ba reflect different sequences of mineral crystallization in the mafic and felsic magma (Chappell et al., 2004). In the mafic magma, plagioclase was the only mineral that contains Ba, and the bulk partition coefficient was much less than unity, so that the Ba contents in the mafic rocks progressively increased. The crystallization of biotite from the felsic magma led to a decrease of Ba contents in the Xiaofeng granitoids.

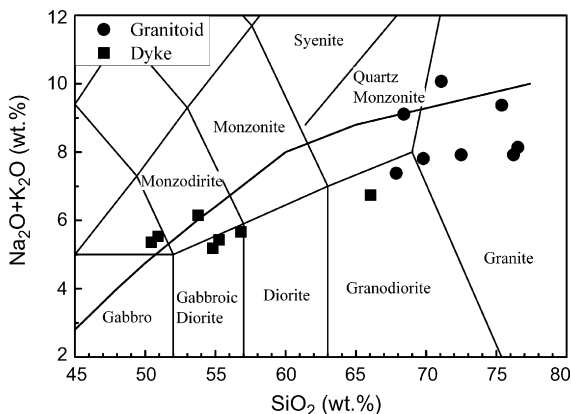


Fig. 4. TAS classification for Neoproterozoic dykes and wall-rock granitoids in the Xiaofeng Suite.

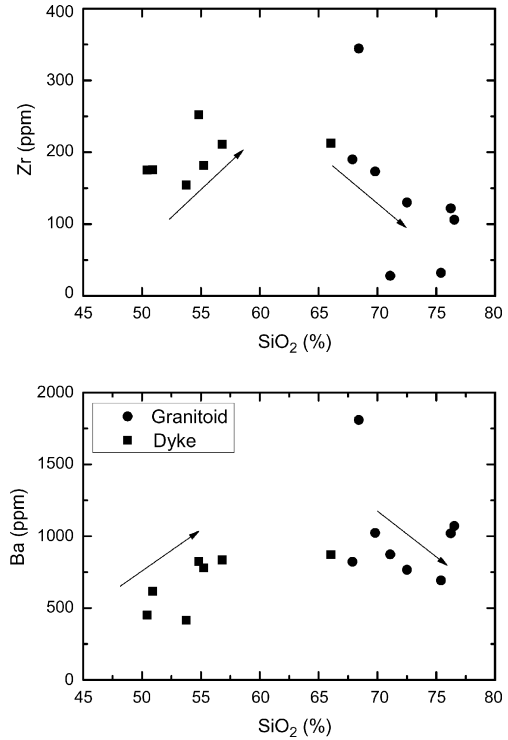


Fig. 5. Variations of Ba and Zr with SiO_2 contents Neoproterozoic dykes and wall-rock granitoids in the Xiaofeng Suite.

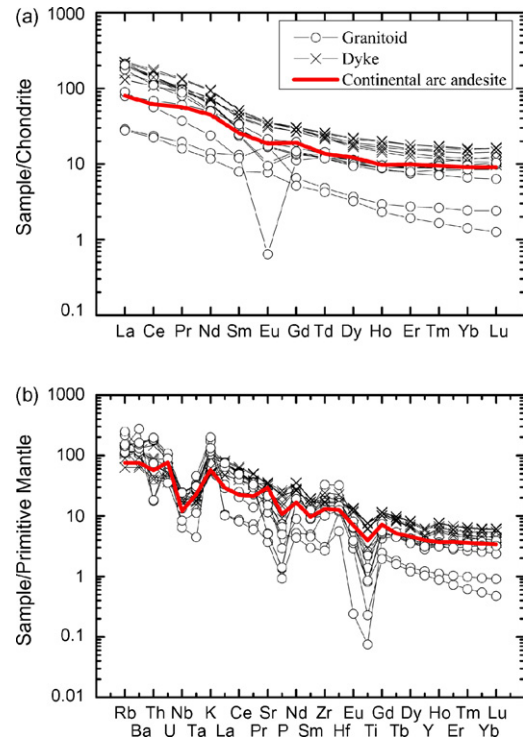


Fig. 6. Normalized patterns of trace elements for Neoproterozoic dykes and wall-rock granitoids in the Xiaofeng Suite. (a) Chondrite-normalized REE patterns (chondrite values are from Sun and McDonough, 1989). (b) Primitive mantle-normalized trace element patterns (primitive mantle values are from McDonough and Sun, 1995). Trace element data for the continental arc are from Kelemen et al. (2003).

Table 2
Oxygen isotope composition of minerals from intrusive rocks at Xiaofeng in the Huangling Batholith

Sample	Rock type	Mineral	$\delta^{18}\text{O}$ (‰)	Pair	$\Delta^{18}\text{O}$ (‰)	T (°C)
04YC01	Gabbro dyke	Pl	8.92			
		Px	4.29	Pl–Px	4.63	197
04YC02	Wall-rock granitoid	Pl	8.80	Zr–Pl	–3.39	442
		Zr	5.41			
		Hb	4.24	Zr–Hb	1.17	dis
		Bi	0.95	Zr–Bi	4.46	dis
04YC03	Diorite dyke	Mt	2.74	Zr–Mt	2.67	624
		Pl	5.37			
		Hb	4.25	Pl–Hb	1.12	909
04YC04	Country-rock granite	Qz	8.71			
		Kfs	6.63	Qz–Kfs	2.08	374
		Pl	6.52	Qz–Pl	2.19	440
		Zr	6.53	Qz–Zr	2.18	948
		Mt	1.76	Qz–Mt	6.95	662
04YC05	Wall-rock granitoid	Qz	8.64			
		Kfs	5.94	Qz–Kfs	2.7	268
		Pl	5.58	Qz–Pl	3.06	297
		Zr	5.92	Qz–Zr	2.72	818
		Mt	1.95	Qz–Mt	6.69	682
04YC06	Diorite dyke	Pl	5.67			
		Hb	5.01	Pl–Hb	0.66	1224
		Mt	2.72	Pl–Mt	2.95	1016
04YC07	Mafic dyke	Hb	5.73			
04YC08	Wall-rock granitoid	Qz	6.58			
		Kfs	6.81	Qz–Kfs	–0.23	1593
		Pl	6.80	Qz–Pl	–0.22	1704
		Zr	5.66	Qz–Zr	0.92	1453
04YC09	Mafic dyke	Pl	6.22			
		Hb	4.38	Pl–Hb	1.84	629
04YC10	Country-rock granite	Qz	9.41			
		Kfs	8.43	Qz–Kfs	0.98	767
		Pl	8.02	Qz–Pl	1.39	677
		Zr	6.19	Qz–Zr	3.22	722
		Mt	3.09	Qz–Mt	6.32	641
		Bi	–0.09	Qz–Bi	9.5	205
04YC11	Diorite dyke	Pl	6.92			
		Hb	5.37	Pl–Hb	1.55	722
		Mt	2.87	Pl–Mt	4.05	734
04YC12	Wall-rock granitoid	Qz	8.95			
		Kfs	7.98	Qz–Kfs	0.97	767
		Pl	7.58	Qz–Pl	1.37	681
04YC13	Wall-rock granitoid	Qz	9.88			
		Kfs	8.87	Qz–Kfs	1.01	744
		Pl	8.69	Qz–Pl	1.19	761
		Gt	5.83	Qz–Gt	4.05	605
04YC14	Diorite dyke	Kfs	7.47	Zr–Kfs	–1.29	1024
		Pl	7.85	Zr–Pl	–1.67	807
		Zr	6.18			
		Hb	5.83	Zr–Hb	0.35	786
04YC15	Mafic dyke	Kfs	7.58	Pl–Kfs	0.4	Dis
		Pl	7.98			
		Mt	3.57	Pl–Mt	4.41	784
04YC16	Mafic dyke	Kfs	6.52	Pl–Kfs	0.66	dis
		Pl	7.18			
04YC17	Intermediate dyke	Pl	7.88			
		Mt	3.79	Pl–Mt	4.09	826

Table 2 (Continued)

Sample	Rock type	Mineral	$\delta^{18}\text{O}$ (‰)	Pair	$\Delta^{18}\text{O}$ (‰)	T (°C)
04YC18	Wall-rock granitoid	Qz	9.00			
		Pl	7.69	Qz–Pl	1.31	706
		Zr	5.90	Qz–Zr	3.1	743
		Hb	4.85	Qz–Hb	4.15	519
04YC19	Country-rock granite	Mt	2.98	Qz–Mt	6.02	740
		Qz	9.27			
		Kfs	8.28	Qz–Kfs	0.99	755
		Pl	7.94	Qz–Pl	1.33	698
04YC20	Mafic dyke	Zr	6.59	Qz–Zr	2.68	826
		Kfs	7.88	Pl–Kfs	−0.96	121
		Pl	6.92			
04YC21	Diorite dyke	Mt	1.15	Pl–Mt	5.77	640
		Hb	4.64	Pl–Hb	2.2	538
04YC22	Wall-rock granitoid	Pl	6.84			
		Qz	7.20	Qz–Pl	−0.3	dis
		Zr	7.99	Qz–Zr	−0.79	dis
		Chl	0.33	Qz–Chl	6.87	253
Continuous section I 05XF01	Country-rock granite	Bi	0.89	Qz–Bi	6.31	355
		Qz	9.05			
		Kfs	8.56	Qz–Kfs	0.49	1178
		Pl	7.92	Qz–Pl	1.13	792
05XF02	Country-rock granite	Zr	6.00	Qz–Zr	3.05	752
		Bi	−0.14	Qz–Bi	9.19	216
		Chl	−1.53	Qz–Chl	10.58	119
		Mt	2.71	Qz–Mt	6.34	711
05XF03	Country-rock granite	Qz	10.15			
		Kfs	9.10	Qz–Kfs	1.05	721
		Pl	8.46	Qz–Pl	1.69	568
		Zr	6.14	Qz–Zr	4.01	603
05XF04	Country-rock granite	Hb	4.81	Qz–Hb	5.34	402
		Qz	10.05			
		Kfs	8.60	Qz–Kfs	1.45	546
		Pl	8.59	Qz–Pl	1.46	646
05XF05	Mafic dyke	Zr	6.48	Qz–Zr	3.57	665
		Chl	−1.52	Qz–Chl	11.57	95
		Qz	10.56			
		Kfs	9.20	Qz–Kfs	1.36	579
05XF06	Mafic dyke	Pl	8.76	Qz–Pl	1.81	533
		Zr	6.31	Qz–Zr	4.26	572
		Ep	0.28	Qz–Ep	10.28	225
		Chl	−0.19	Qz–Chl	10.75	114
05XF07	Mafic dyke	Lim	−2.37	Qz–Lim	12.93	373
		Pl	8.63			
		Hb	4.27	Pl–Hb	4.36	251
		Ep	−1.06	Pl–Ep	8.44	dis
05XF08	Mafic dyke	Pl	7.38			
		Mt	2.08	Pl–Mt	5.98	622
		Ep	−1.30	Pl–Ep	9.36	dis
05XF09	Mafic dyke	Pl	7.12			
		Ep	−1.03	Pl–Ep	8.15	dis
05XF09	Mafic dyke	Pl	6.90			
		Ep	0.87	Pl–Ep	6.03	25

Table 2 (Continued)

Sample	Rock type	Mineral	$\delta^{18}\text{O}$ (‰)	Pair	$\Delta^{18}\text{O}$ (‰)	T (°C)
05XF10	Mafic dyke	Pl	6.57			
		Hb	3.35	Pl–Hb	3.22	365
		Mt	2.28	Pl–Mt	4.29	800
		Ep	−0.99	Pl–Ep	7.56	dis
05XF11	Wall-rock granitoid	Qz	7.89			
		Pl	6.56	Qz–Pl	1.33	698
		Zr	5.82	Qz–Zr	2.07	980
		Ep	0.84	Qz–Ep	7.06	367
05XF12	Wall-rock granitoid	Qz	8.20			
		Pl	6.74	Qz–Pl	1.46	646
		Zr	6.06	Qz–Zr	2.14	960
		Bi	0.26	Qz–Bi	7.94	266
05XF13	Wall-rock granitoid	Ilm	−3.71	Qz–Ilm	11.91	374
		Qz	8.36			
		Pl	6.15	Qz–Pl	2.21	438
		Zr	6.11	Qz–Zr	2.25	930
05XF14	Wall-rock granitoid	Ep	1.20	Qz–Ep	7.16	361
		Qz	8.17			
		Kfs	6.96	Qz–Kfs	1.21	642
		Pl	6.23	Qz–Pl	0.73	1054
05XF15	Wall-rock granitoid	Zr	5.51	Qz–Zr	0.73	1572
		Ilm	−3.62	Qz–Ilm	9.12	490
		Qz	7.85			
		Kfs	7.61	Qz–Kfs	0.24	1572
05XF16	Country-rock granite	Pl	6.67	Qz–Pl	1.19	762
		Zr	5.44	Qz–Zr	2.41	889
		Px	1.67	Qz–Px	6.18	318
		Qz	8.82			
05XF17	Mafic dyke	Kfs	8.51	Qz–Kfs	0.31	1440
		Pl	7.91	Qz–Pl	0.91	920
		Zr	5.49	Qz–Zr	3.33	703
		Hb	3.98	Qz–Hb	4.84	446
		Ep	−0.80	Qz–Ep	9.62	248
		Chl	−1.84	Qz–Chl	10.66	116
		Hb	4.20	Pl–Hb	2.52	473
05XF18	Wall-rock granitoid	Pl	6.72			
		Qz	9.59			
		Kfs	6.00	Qz–Kfs	3.60	168
		Pl	6.33	Qz–Pl	3.26	272
		Zr	5.44	Qz–Zr	4.16	584
		Ep	−0.59	Qz–Ep	10.18	229
05XF19	Wall-rock granitoid	Mt	2.11	Qz–Mt	7.49	623
		Qz	10.16			
		Kfs	7.71	Qz–Kfs	2.46	304
		Pl	7.68	Qz–Pl	2.49	382
		Zr	6.41	Qz–Zr	3.76	637
05XF20	Wall-rock granitoid	Sph	5.13	Qz–Sph	5.03	921
		Ep	−0.03	Qz–Ep	10.19	228
		Mt	2.35	Qz–Mt	7.81	602
		Qz	10.02			
05XF21	Wall-rock granitoid	Kfs	7.77	Qz–Kfs	2.25	340
		Pl	7.33	Qz–Pl	2.69	349
		Zr	6.65	Qz–Zr	3.38	695
		Gt	6.27	Qz–Gt	3.76	644
		Hb	5.39	Qz–Hb	4.64	397
		Bi	1.08	Qz–Bi	8.94	225
		Px	1.72	Qz–Px	8.30	211
		Mt	2.13	Qz–Mt	7.89	597

Table 2 (Continued)

Sample	Rock type	Mineral	$\delta^{18}\text{O}$ (‰)	Pair	$\Delta^{18}\text{O}$ (‰)	T (°C)
05XF21	Wall-rock granitoid	Qz	9.76			
		Kfs	6.57	Qz–Kfs	3.19	208
		Pl	8.01	Qz–Pl	1.76	547
		Zr	6.41	Qz–Zr	3.35	700
		Hb	5.54	Qz–Hb	4.22	511
		Ep	−0.37	Qz–Ep	10.13	230
05XF22	Wall-rock granitoid	Mt	3.26	Qz–Mt	6.50	698
		Qz	9.71			
		Kfs	6.90	Qz–Kfs	2.81	253
		Pl	6.50	Qz–Pl	3.21	278
		Zr	6.50	Qz–Zr	3.21	723
		Bi	−0.32	Qz–Bi	10.03	187
05XF23	Mafic dyke	Mt	2.21	Qz–Mt	7.50	623
		Ep	0.04	Pl–Ep	6.18	20
05XF24	Mafic dyke	Pl	6.22			
		Hb	3.82	Pl–Hb	2.14	552
		Ep	−1.01	Pl–Ep	6.96	dis
05XF25A	Mafic dyke	Pl	5.71			
		Hb	6.39	Pl–Hb	−0.68	dis
05XF25B	Wall-rock granitoid	Qz	9.38			
		Kfs	6.73	Qz–Kfs	2.65	275
		Pl	6.54	Qz–Pl	2.84	327
		Hb	5.58	Qz–Zr	3.81	562
05XF26	Wall-rock granitoid	Mt	2.62	Qz–Mt	6.76	677
		Qz	9.39			
		Kfs	6.23	Qz–Kfs	3.16	211
		Pl	6.80	Qz–Pl	2.59	365
05XF27	Wall-rock granitoid	Zr	5.80	Qz–Zr	3.59	662
		Qz	9.54			
		Kfs	7.44	Qz–Kfs	2.10	370
		Pl	7.60	Qz–Pl	1.95	496
05XF28	Wall-rock granitoid	Zr	6.56	Qz–Zr	2.98	765
		Hb	5.55	Qz–Hb	3.99	538
		Qz	9.80			
		Kfs	7.50	Qz–Kfs	2.30	331
05XF28	Wall-rock granitoid	Pl	6.86	Qz–Pl	2.95	311
		Zr	6.80	Qz–Zr	3.01	760
		Hb	5.96	Qz–Hb	3.85	556
		Bi	0.58	Qz–Bi	9.23	214
		Mt	1.68	Qz–Mt	8.12	583

As shown in Fig. 6, the dykes and granitoid rocks of the Xiaofeng Suite have similar patterns of REE and trace element partition. Both dykes and granitoids are characterized by LREE-enriched patterns. The dykes show less fractionated REE patterns, with $(\text{La}/\text{Yb})_N$ ratios of 8.1–20.9 that are lower than 12.0–46.9 for the granitoids (except sample 04YC13). Sample 04YC13 has a relatively flat REE pattern with a $(\text{La}/\text{Yb})_N$ ratios of 2.5 and strongly negative Eu anomaly. This is because this granitoid is highly evolved with extremely low content of Ca for which Eu usually substitutes and contains garnet. The occurrence of garnet which is enriched in HREE relative to LREE is another reason for its flat REE pattern. While most of the granitoids have significant negative Eu anomaly, the dykes do not exhibit considerable Eu anomaly. All the samples have similar trace element distribution patterns with enrichment of Rb, Ba,

Th, U, K but depletion of Nb, Ta and Ti. No depletion of Sr is observed. These patterns are generally similar to those for the average continental arc andesites (Kelemen et al., 2003), but the LILE are slightly more enriched than the continental arc. Such patterns are common for the continental crust that is normally interpreted to originate from the geochemical evolution of arc-derived magmas (Rudnick, 1995; Taylor and McLennan, 1995; Hawkesworth and Kemp, 2006; Wu et al., 2006a).

4.2. Mineral O isotopes

Mineral O isotopic data for the Xiaofeng rocks are listed in Table 2. As a whole, $\delta^{18}\text{O}$ values are 6.58–10.56‰ for quartz, 5.94–9.20‰ for K-feldspar, 8.37–8.76‰ for plagioclase, 5.41–6.80‰ for zircon (one exception at 7.99‰),

3.35–6.39‰ for hornblende, 1.15–3.79‰ for magnetite, –0.32 to 1.08‰ for biotite, –1.84 to 0.33‰ for chlorite, and –1.30 to 0.28‰ for epidote. Generally, the $\delta^{18}\text{O}$ values for most minerals from the wall-rock granitoids and the country-rock granites in the Xiaofeng area are undistinguishable. But the $\delta^{18}\text{O}$ ranges for quartz, K-feldspar, plagioclase are different from each other. The country-rock granites have relatively higher $\delta^{18}\text{O}$ values but a smaller variation. For example, $\delta^{18}\text{O}$ values for quartz are 6.58–10.16‰ for the granitoids, but 8.71–10.56‰ for the country-rock granites. In either case, the quartz $\delta^{18}\text{O}$

values of 6.58–10.56‰ for the Xiaofeng intrusions are consistent with those for I-type granite (O’Neil and Chappell, 1977). However, the low $\delta^{18}\text{O}$ values of –1.84 to 1.11‰ for hydroxyl-bearing minerals such as biotite, chlorite and epidote indicate high-T hydrothermal alteration by surface water during magma emplacement (Taylor, 1977).

Mineral-pair O isotopic temperatures are calculated using the fractionation O curves of Zheng (1993a,b, 1995), assuming preservation of isotope equilibration at the scale of sample measurement. Judgment and interpretation of O isotope equilibrium

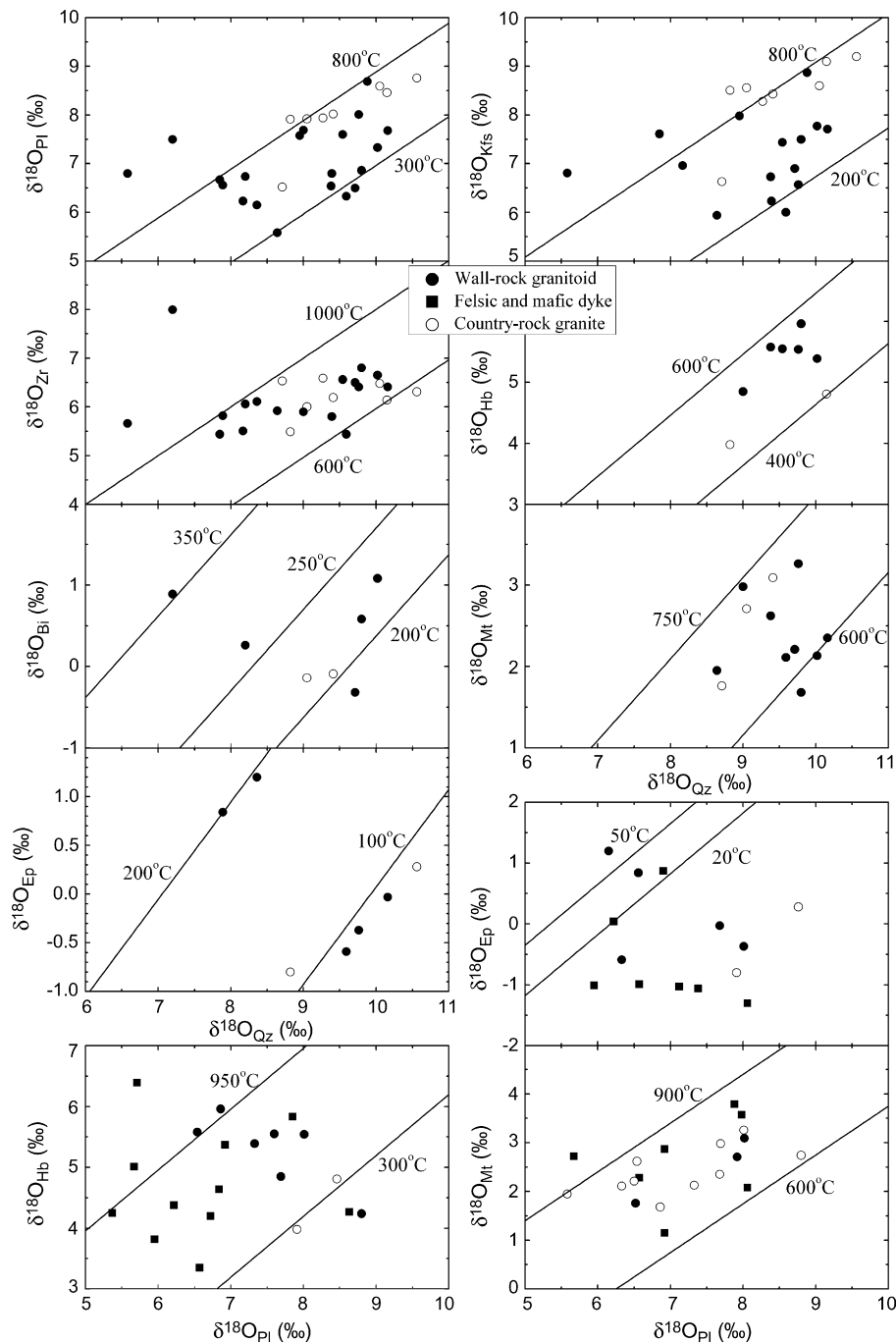


Fig. 7. Mineral-pair O isotope plots for igneous rocks at Xiaofeng. Isotherms are calculated using the O isotope fractionation factors of Zheng (1993a,b, 1995).

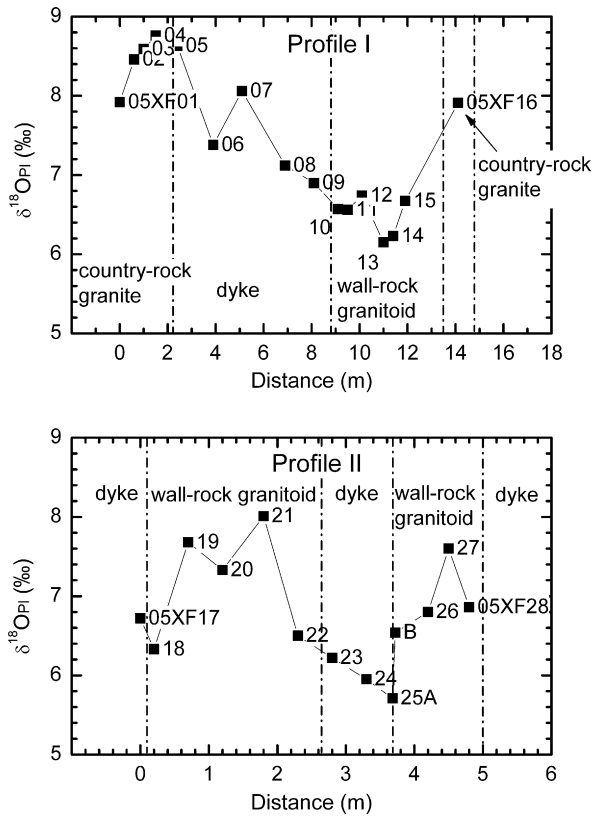


Fig. 8. Variation of plagioclase $\delta^{18}\text{O}$ values for two profiles in the Xiaofeng area.

or disequilibrium between coexisting minerals are based on measured fractionation values and resultant sequence of O isotope temperatures in combination with rates of O diffusion in concerned minerals and corresponding sequence of closure temperatures (Giletti, 1986; Zhao et al., 2004; Chen et al., 2007a). Isotherms are constructed for mineral-pair $\delta^{18}\text{O}$ values (Fig. 7), with equilibrium fractionations having slopes equal to unity. Most rock-forming minerals lie in the state of O isotope equilibrium. However, minerals susceptible to secondary alteration such as biotite, chlorite and epidote are not equilibrated with resistant minerals. The relatively lower temperatures are calculated by the hydroxyl-bearing minerals, implying hydrothermal alteration after the magma crystallization.

Two continuous profiles were sampled for O isotope analyses in order to study hydrothermal activity during emplacement of the Xiaofeng dykes. Because plagioclase is the only mineral present in both wall-rock granitoids and the mafic dykes, its $\delta^{18}\text{O}$ values are plotted in Fig. 8 to show the continuous variation in O isotope ratios along the profiles. The first profile (Fig. 8a) is about 15 m in length, from the country-rock granite, through the Xiaofeng dyke and wall-rock granitoid, to the country-rock granite of the other side. This profile exhibits that the Xiaofeng intrusions have lower $\delta^{18}\text{O}$ values than the country rocks. This implies that the country rocks were altered by low-T surface-hydrothermal fluid, a common feature for ancient rocks. The second profile (Fig. 8b) is about 5 m in length, but straddle across two mafic dykes and two wall-rock granitoids of the Xiaofeng Suite. The $\delta^{18}\text{O}$ values for plagioclase in the wall-rock granitoids

show a significant decrease at the contact between the granitoids and mafic dykes. This points to small-scale high-T water-rock interaction during intrusion of the Xiaofeng dykes.

4.3. Zircon U–Pb geochronology

Zircons from rocks of the Xiaofeng Suite have lengths of ~ 100 to ~ 300 μm except zircons from felsic dyke 04YC11 that are relatively smaller with lengths of 50–200 μm . Most zircons from felsic rocks (04YC02, 04YC05, 04YC130, 04YC11) are long prismatic or short prismatic with a few having equant forms. Concentric zoning or parallel zoning is developed in these zircons (Fig. 9a–c). Zircons from mafic dyke 05XF23 have irregular morphologies with broad parallel growth zonings (Fig. 9d). Three wall-rock granitoids (04YC02, 04YC05, 04YC13), a felsic dyke (04YC11) and a mafic dyke (05XF23) were measured for zircon U–Pb isotopes by the SHRIMP and LA-ICPMS methods. The results are listed in Tables 3 and 4, respectively.

Twenty-four spots on 24 zircons were analyzed for granitoid 04YC02 (Table 4). Of the 24 grains analyzed, 18 grains yield $^{206}\text{Pb}/^{238}\text{U}$ ages around 800 Ma with a weighted mean at 797 ± 5 Ma (MSWD = 3.2), interpreted as the crystallization age. If only considering the most concordant three analyses, a weighed mean $^{206}\text{Pb}/^{238}\text{U}$ age of 794 ± 7 Ma is obtained to be identical with the crystallization age within analytical errors. The other six grains have younger apparent ages, reflecting Pb loss in later events (Fig. 10a). The 18 analyses form a discordia intercept age of 797 ± 7 Ma (MSWD = 3.3), identical with the mean $^{206}\text{Pb}/^{238}\text{U}$ age. A few highly discordant analyses show elevated $^{207}\text{Pb}/^{235}\text{U}$ ratios but similar $^{206}\text{Pb}/^{238}\text{U}$ ratios with those concordant analyses. The other six analyses with younger apparent ages plot near an array (dashed line in Fig. 10a) which has the trend to intersect with the concordia curve at the Triassic, pointing to the influence of Triassic collision.

Totally 22 spots on 20 grains (Table 4) were analyzed for granitoid 04YC05 (Fig. 10b). The results are quite similar to those for sample 04YC02. Seventeen analyses show $^{206}\text{Pb}/^{238}\text{U}$ ages around 800 Ma, yielding a weighted mean of 799 ± 2 Ma (MSWD = 1.12). These 17 analyses defined a discordia that intersects the concordia curve at 801 ± 3 Ma (MSWD = 0.92). The other five analyses with different degrees of Pb loss have the trend to intersect at Triassic.

Zircon grains extracted from granitoid 04YC13 are very limited, thus not displayed in Fig. 9. Both SHRIMP (Table 3) and LA-ICPMS (Table 4) were used for U–Pb analysis of this sample. Some zircons have discordant ages about 800 Ma. The others have much older apparent ages. Altogether they form a discordia with intercept ages at 2979 ± 140 and 775 ± 170 Ma, respectively (Fig. 10c). There are two possibilities to interpret the data: one is that the older zircons are captured from the country rocks during granite emplacement; the other is that the Archean precursor was partially melted so that both restite and new crystallized zircons are present in this sample.

Zircons from felsic dyke 04YC11 were dated by the SHRIMP technique (Table 3). Four analyses on four zircons yield similar apparent $^{206}\text{Pb}/^{238}\text{U}$ ages with a weighted mean of 806 ± 12 Ma,

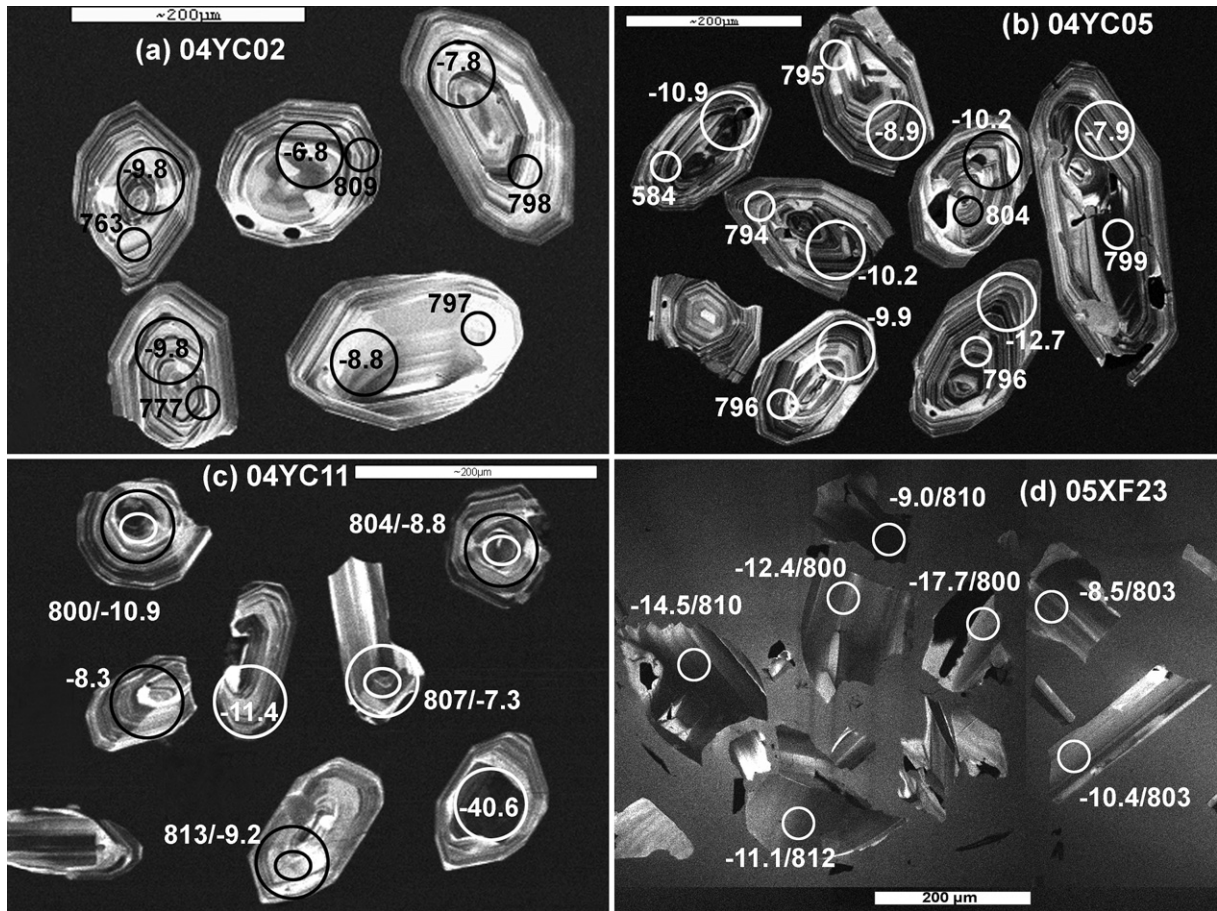


Fig. 9. Zircon CL images with $\epsilon_{\text{Hf}}(t)$ values and U–Pb ages for granitoids (a and b), felsic dyke (c) and mafic dyke (d) in the Xiaofeng Suite.

interpreted as the crystallization age. A discordia defined by the data intersects the concordia curve at 804 ± 6 Ma (Fig. 10d). It is consistent with the results obtained by Li et al. (2004b) from a felsic dyke in the same outcrop.

Twenty-four analyses were made on mafic dyke 05XF23 by the LA-ICPMS method. Most analyses are concordant or near concordant. Only a few are highly discordant with elevated $^{207}\text{Pb}/^{235}\text{U}$ ratios. All analyses yield similar $^{206}\text{Pb}/^{238}\text{U}$ age from 800 to 812 Ma (Fig. 10e), with a weighted mean of 806 ± 4 Ma (MSWD = 0.16). They form a discordia intersects the concordia curve at 807 ± 5 Ma. The consistence in the U–Pb ages between the mafic and felsic dykes demonstrate that they formed simultaneously.

4.4. Whole-rock Sr–Nd isotopes

Five samples, three wall-rock granitoids (04YC02, 04YC05, 04YC13) and two dykes (04YC11, 04YC20), were measured for their Rb–Sr and Sm–Nd isotopes (Table 5). Additional four samples from the two profiles, including one wall-rock granitoid (05XF13) and three dykes (05XF13, 05XF23, 05XF24), were analyzed for their Sm–Nd isotopes. Initial Sr and Nd isotope ratios are calculated by assuming $t = 800$ Ma.

The granitoids have variably low $(^{87}\text{Sr}/^{86}\text{Sr})_i$ values at their crystallization age. Two dykes (04YC11 and 04YC20) have similar $(^{87}\text{Sr}/^{86}\text{Sr})_i$ values of about 0.706. The large variations in $^{87}\text{Rb}/^{86}\text{Sr}$ and $(^{87}\text{Sr}/^{86}\text{Sr})_i$ suggest that their Rb–Sr isotopic systems were disturbed variably after their crystallization (Zheng, 1989).

Sm–Nd isotope system is generally accepted to be more robust than Rb–Sr isotope system, thus can record information on source materials. Totally nine samples of the felsic and mafic rocks have consistent $^{143}\text{Nd}/^{144}\text{Nd}$ ratios of 0.511415–0.511926, implying that they have the similar source materials. Corresponding $\epsilon_{\text{Nd}}(t)$ values range from -10.6 to -6.4 (except sample 04YC13 which has a too high $^{147}\text{Sm}/^{144}\text{Nd}$ ratio), suggesting they are derived from ancient rocks. Another feature of the Sm–Nd isotopes in the Xiaofeng rocks is that $\epsilon_{\text{Nd}}(t)$ values for mafic rocks are slightly higher than those for the felsic rocks. Because the $^{147}\text{Sm}/^{144}\text{Nd}$ ratios for these rocks deviate significantly from 0.118 for the average continental crust (Jahn and Condie, 1995), single-stage Nd model ages (T_{DM1}) are affected by Sm/Nd fractionation. Two-stage Nd model ages (T_{DM2}) are calculated following the formulation of Liew and Hofmann (1988) relative to the average continental crust of Jahn and Condie (1995). Except for sample 04YC13, the rocks from the Xiaofeng intrusions have two-stage Nd model ages of

Table 3
SHRIMP zircon U–Pb isotopic data for intrusive rocks at Xiaofeng in the Huangling Batholith

Spot	²⁰⁶ Pb _c (%)	U (ppm)	Th (ppm)	²³² Th/ ²³⁸ U	²³⁸ U/ ²⁰⁶ Pb* (ppm)	²⁰⁶ Pb*/ ²⁰⁶ Pb* ±%	²⁰⁷ Pb*/ ²⁰⁶ Pb* ±%	²⁰⁷ Pb*/ ²³⁵ U ±%	²⁰⁶ Pb*/ ²³⁸ U ±%	±%	Err. corr.	Age (Ma)	²⁰⁷ Pb/ ²⁰⁶ Pb	²⁰⁸ Pb/ ²³² Th			
Felsic dyke 04YC11																	
1.1	1.21	110	157	1.48	12.6	7.57	1.4	0.0726	2.3	1.3223	2.4	0.1321	1.4	0.703	800 ± 12	1003 ± 47	789 ± 29
2.1	0.46	148	201	1.41	17.0	7.48	1.3	0.0663	1.9	1.2222	2.1	0.1337	1.3	0.814	809 ± 11	816 ± 40	807 ± 28
3.1	0.73	142	224	1.63	16.9	7.53	3.3	0.0673	2.2	1.2323	2.3	0.1328	1.5	0.742	804 ± 13	847 ± 46	842 ± 30
4.1	13.10	59	64	1.12	8.61	7.43	1.7	0.1148	3.3	2.1289	3.5	0.1345	1.7	0.353	813 ± 15	1877 ± 59	1850 ± 70
Wall-rock granitoid 04YC13																	
1.1	0.54	199	173	0.90	24.8	6.94	2.7	0.0657	4.0	1.301	4.8	0.1436	2.7	0.558	865 ± 22	797 ± 83	889 ± 36
2.1	0.22	206	194	0.97	25.0	7.12	3.3	0.0663	2.3	1.294	4.0	0.1415	3.3	0.818	853 ± 26	816 ± 49	860 ± 32
3.1	0.58	270	184	0.71	40.0	5.82	2.5	0.0807	2.5	1.912	3.7	0.1718	2.7	0.725	1022 ± 25	1214 ± 50	932 ± 31

2.00–2.34 Ga (Table 5). The Sm–Nd isotopic result for sample 04YC13 is meaningless because it experienced strong Sm–Nd fractionation.

4.5. Zircon Lu–Hf isotopes

Zircon Lu–Hf isotopes were analyzed for the four U–Pb dated samples and the results are listed in Table 6. The analyses were taken on the same spots for U–Pb dating or the same nature of domain close to the spots. Corresponding U–Pb analysis spots are listed in the second row of Table 6. Because the Huangling Batholith is mainly composed of TTG rocks (Li et al., 2003b; Ling et al., 2006), they are generally thought to form by partial melting of mafic rocks, either subducted slabs (e.g., Defant and Drummond, 1990; Martin, 1999) or thickened lower crust (e.g., Smithies, 2000; Rapp et al., 2003). Thus we used a ¹⁷⁶Lu/¹⁷⁷Hf of 0.022 for average mafic rocks (Amelin et al., 2000) in calculating two-stage Hf model ages for the wall-rock granitoids from the Xiaofeng Suite.

Fifteen Lu–Hf isotope analyses were made on zircons from granitoid 04YC02. ¹⁷⁶Hf/¹⁷⁷Hf ratios are quite homogeneous, ranging from 0.281981 to 0.282119. $\epsilon_{\text{Hf}}(t)$ values calculated at $t=800$ Ma are from –10.8 to –6.0, with a weighted mean of –8.3 (Fig. 11a). Two-stage Hf model ages range from 2.7 to 3.0 Ga, with a weighted mean at 2.8 Ga (Fig. 12a). This implies that the source material of the granitoid was extracted from the very ancient crust that formed by crust–mantle differentiation in the Mesoarchean.

Fifteen Lu–Hf isotope analyses were made on zircons from granitoid 04YC05. The results are very similar to those for granitoid 04YC02. $\epsilon_{\text{Hf}}(t)$ values ($t=800$ Ma) range from –12.9 to –7.9, with a weighted mean of –10.5 (Fig. 11b). Two-stage Hf model ages are 2.8–3.2 Ga, with a weighted mean of 3.0 Ga (Fig. 12b).

Although the zircons are very scarce, Lu–Hf isotopic data for granitoid 04YC13 is quite complicated. A few zircons with Archean ages have very low ¹⁷⁶Hf/¹⁷⁷Hf ratios (Table 6). Because their U–Pb ages are highly discordant, $\epsilon_{\text{Hf}}(t)$ values are calculated using the upper intercept age of 2.98 Ga for these zircons. This yields variable $\epsilon_{\text{Hf}}(t)$ values of –5.1 to 3.2 (Table 6). For the zircons with Neoproterozoic U–Pb ages, $\epsilon_{\text{Hf}}(t)$ values are calculated using an assumed age of 800 Ma because the lower intercept age is poorly defined, and two-stage Hf model ages are calculated using a ¹⁷⁶Lu/¹⁷⁷Hf of 0.022. This results in $\epsilon_{\text{Hf}}(t)$ values of –12.0 to –9.1 with T_{DM2} values of 2.88–3.14 Ga (Table 6). While ¹⁷⁶Hf/¹⁷⁷Hf ratios for the ancient zircons fall in the range of the Kongling rocks (Zhang et al., 2006a), ¹⁷⁶Hf/¹⁷⁷Hf ratios for the younger zircons are similar to the other granitoids in the Xiaofeng Suite (Table 6). Thus, the zircons with Hf isotopes similar to the Kongling rocks might be captured from the country rocks or brought up from the source rocks.

Fifteen Lu–Hf isotope analyses were made on zircons from felsic dyke 04YC11. Except for one analysis on the core of a single zircon, the all other spots have ¹⁷⁶Hf/¹⁷⁷Hf ratios of 0.281966–0.282082. $\epsilon_{\text{Hf}}(t)$ values calculated at $t=800$ Ma are –10.9 to –7.3, with a weighted mean of –9.0 (Fig. 11c). Two-

Table 4
LA-ICPMS zircon U–Pb isotopic data for intrusive rocks at Xiaofeng in the Huangling Batholith

No	Pb	Th	U	Th/U	Isotopic ratios						Apparent ages (Ma)						Com Pb%				
					²⁰⁷ Pb/ ²⁰⁶ Pb	2σ	²⁰⁷ Pb/ ²³⁵ U	2σ	²⁰⁶ Pb/ ²³⁸ U	2σ	²⁰⁸ Pb/ ²³² Th	2σ	²⁰⁷ Pb/ ²⁰⁶ Pb	2σ	²⁰⁷ Pb/ ²³⁵ U	2σ		²⁰⁶ Pb/ ²³⁸ U	2σ	²⁰⁸ Pb/ ²³² Th	2σ
Wall-rock granitoid 04YC02																					
1.1	14	75	67	1.13	0.06696	0.00109	1.21691	0.01668	0.13180	0.00086	0.03921	0.00028	837	18	808	8	798	5	777	5	0.0
2.1	15	96	70	1.37	0.06789	0.00123	1.23236	0.01948	0.13165	0.00091	0.04029	0.00031	865	21	815	9	797	5	798	6	0.0
3.1	27	350	187	1.87	0.08680	0.00269	1.60001	0.04675	0.13369	0.00151	0.03470	0.00044	1356	39	970	18	809	9	689	9	0.0
4.1	13	80	58	1.37	0.09120	0.00291	1.58091	0.04849	0.12572	0.00109	0.03707	0.00025	1451	62	963	19	763	6	736	5	2.1
5.1	15	83	78	1.07	0.07081	0.00092	1.25042	0.01225	0.12808	0.00074	0.03887	0.00022	952	11	824	6	777	4	771	4	0.0
6.1	19	165	105	1.58	0.06850	0.00246	1.23188	0.04243	0.13043	0.00153	0.03071	0.00046	884	52	815	19	790	9	611	9	0.0
7.1	17	130	100	1.30	0.07605	0.00239	1.39203	0.04142	0.13275	0.00143	0.02241	0.00031	1096	42	886	18	804	8	448	6	0.0
8.1	25	186	129	1.45	0.07417	0.00205	1.34307	0.03582	0.13134	0.00096	0.03960	0.00022	1046	57	865	16	795	5	785	4	0.6
9.1	37	329	174	1.89	0.07531	0.00124	1.38401	0.01928	0.13329	0.00089	0.03593	0.00023	1077	17	882	8	807	5	713	4	0.0
10.1	20	221	115	1.92	0.06782	0.00194	1.09211	0.02927	0.11679	0.00113	0.03395	0.00039	863	39	750	14	712	7	675	8	0.0
11.1	23	188	111	1.70	0.06527	0.00296	1.15876	0.05144	0.12876	0.00116	0.03938	0.00024	783	98	781	24	781	7	781	5	3.2
12.1	23	192	117	1.65	0.10110	0.00193	1.82490	0.03062	0.13091	0.00104	0.04860	0.00041	1644	19	1054	11	793	6	959	8	0.0
13.1	10	115	63	1.83	0.07778	0.00170	1.08689	0.02154	0.10136	0.00081	0.01905	0.00018	1141	27	747	10	622	5	381	4	0.0
14.1	22	179	118	1.52	0.07333	0.00211	1.33098	0.03600	0.13165	0.00131	0.02593	0.00030	1023	39	859	16	797	7	517	6	0.0
15.1	22	165	112	1.48	0.06664	0.00262	1.21528	0.04594	0.13227	0.00166	0.03810	0.00058	827	58	808	21	801	9	756	11	0.0
16.1	25	189	124	1.52	0.08900	0.00453	1.41898	0.07029	0.11563	0.00134	0.03418	0.00030	1404	100	897	30	705	8	679	6	6.0
17.1	18	122	85	1.44	0.07214	0.00108	1.30128	0.01592	0.13084	0.00082	0.03679	0.00023	990	15	846	7	793	5	730	4	0.0
18.1	44	323	228	1.42	0.07383	0.00126	1.35940	0.01987	0.13355	0.00091	0.03936	0.00028	1037	19	872	9	808	5	780	5	0.0
19.1	21	145	111	1.31	0.06819	0.00107	1.25244	0.01625	0.13320	0.00085	0.04030	0.00026	874	16	825	7	806	5	799	5	0.0
20.1	20	164	191	0.86	0.07681	0.00173	0.65783	0.01335	0.06211	0.00049	0.02569	0.00025	1116	28	513	8	388	3	513	5	0.0
21.1	37	321	190	1.69	0.08182	0.00152	1.47224	0.02399	0.13051	0.00096	0.02741	0.00021	1241	20	919	10	791	5	547	4	0.0
22.1	38	310	231	1.34	0.12576	0.00422	2.29406	0.07246	0.13230	0.00187	0.05606	0.00093	2040	36	1210	22	801	11	1102	18	0.0
23.1	33	252	157	1.61	0.06929	0.00110	1.27667	0.01700	0.13363	0.00086	0.03894	0.00024	907	17	835	8	809	5	772	5	0.0
24.1	36	293	180	1.62	0.09191	0.00143	1.50928	0.01923	0.11910	0.00079	0.03532	0.00023	1466	14	934	8	725	5	702	4	0.0
Wall-rock granitoid 04YC05																					
1.1	26	234	96	2.43	0.09726	0.00131	1.76869	0.01808	0.13187	0.00079	0.03907	0.00021	1572	11	1034	7	799	4	775	4	0.0
2.1	14	88	80	1.10	0.06951	0.00117	1.26014	0.01791	0.13146	0.00086	0.03684	0.00027	914	19	828	8	796	5	731	5	0.0
3.1	23	189	115	1.65	0.06756	0.00089	1.23733	0.01209	0.13282	0.00075	0.03539	0.00018	855	11	818	5	804	4	703	4	0.0
4.1	33	266	165	1.61	0.07648	0.00123	1.38528	0.01846	0.13135	0.00085	0.03837	0.00025	1108	16	883	8	796	5	761	5	0.0
5.1	31	235	164	1.44	0.06879	0.00091	1.24379	0.01244	0.13113	0.00075	0.03598	0.00019	892	12	821	6	794	4	714	4	0.0
6.1	40	411	272	1.51	0.07571	0.00086	0.98966	0.00722	0.09481	0.00050	0.02535	0.00011	1087	7	699	4	584	3	506	2	0.0
7.1	26	221	134	1.65	0.06920	0.00097	1.25271	0.01377	0.13129	0.00077	0.03218	0.00018	905	13	825	6	795	4	640	4	0.0
8.1	32	258	159	1.62	0.06976	0.00106	1.26379	0.01557	0.13139	0.00081	0.03853	0.00024	921	15	830	7	796	5	764	5	0.0
9.1	16	90	79	1.15	0.07060	0.00098	1.29216	0.01382	0.13273	0.00077	0.03825	0.00022	946	13	842	6	803	4	759	4	0.0
10.1	25	251	137	1.83	0.07267	0.00147	1.32382	0.02399	0.13213	0.00098	0.03010	0.00024	1005	25	856	10	800	6	599	5	0.0
11.1	20	204	89	2.30	0.06967	0.00119	1.27318	0.01858	0.13255	0.00087	0.03753	0.00024	919	19	834	8	802	5	745	5	0.0
12.1	25	207	148	1.40	0.07647	0.00237	1.40246	0.04117	0.13302	0.00137	0.04086	0.00055	1107	42	890	17	805	8	809	11	0.0
13.1	47	441	284	1.55	0.07363	0.00100	1.07017	0.01109	0.10541	0.00061	0.03129	0.00017	1031	12	739	5	646	4	623	3	0.0
14.1	21	126	102	1.24	0.09022	0.00206	1.61354	0.03511	0.12971	0.00089	0.03829	0.00022	1430	45	975	14	786	5	759	4	1.7

Table 4 (Continued)

No	Pb	Th	U	Th/U	Isotopic ratios						Apparent ages (Ma)						Com Pb%				
					$^{207}\text{Pb}/^{206}\text{Pb}$	2σ	$^{207}\text{Pb}/^{235}\text{U}$	2σ	$^{206}\text{Pb}/^{238}\text{U}$	2σ	$^{208}\text{Pb}/^{232}\text{Th}$	2σ	$^{207}\text{Pb}/^{206}\text{Pb}$	2σ	$^{207}\text{Pb}/^{235}\text{U}$	2σ		$^{206}\text{Pb}/^{238}\text{U}$	2σ	$^{208}\text{Pb}/^{232}\text{Th}$	2σ
15.1	23	146	111	1.31	0.06875	0.00088	1.25104	0.01171	0.13198	0.00073	0.03887	0.00020	891	11	824	5	799	4	771	4	0.0
16.1	34	386	230	1.68	0.07452	0.00089	0.92830	0.00749	0.09035	0.00048	0.02437	0.00011	1056	8	667	4	558	3	487	2	0.0
16.2	67	1132	433	2.61	0.08940	0.00100	1.02782	0.00729	0.08339	0.00044	0.02443	0.00010	1413	6	718	4	516	3	488	2	0.0
17.1	28	208	129	1.61	0.07280	0.00092	1.33287	0.01215	0.13279	0.00074	0.04220	0.00021	1008	10	860	5	804	4	835	4	0.0
18.1	35	274	193	1.42	0.07230	0.00130	1.32151	0.02066	0.13258	0.00091	0.03989	0.00031	994	21	855	9	803	5	791	6	0.0
19.1	41	431	544	0.79	0.09375	0.00110	0.66526	0.00516	0.05147	0.00027	0.02274	0.00012	1503	7	518	3	324	2	454	2	0.0
19.2	42	373	269	1.39	0.07428	0.00364	1.36527	0.06488	0.13332	0.00207	0.04433	0.00092	1049	71	874	28	807	12	877	18	0.0
20.1	30	226	160	1.42	0.06885	0.00122	1.26176	0.01936	0.13293	0.00089	0.03974	0.00030	894	21	829	9	805	5	788	6	0.0
Wall-rock granitoid 04YC13																					
1.1	212	108	468	0.23	0.20705	0.00214	13.35879	0.08175	0.46791	0.00265	0.12114	0.00078	2542	5	2705	6	2474	12	2311	14	0.0
1.2	248	251	513	0.49	0.19943	0.00193	14.25898	0.10933	0.51855	0.00307	0.14164	0.00081	2473	18	2767	7	2693	13	2677	14	0.2
3.1	23	93	137	0.68	0.06832	0.00094	1.24863	0.01348	0.13254	0.00080	0.03655	0.00026	105	17	823	6	802	5	726	5	0.0
4.1	37	99	60	1.65	0.21348	0.00261	10.43373	0.09444	0.35446	0.00248	0.15154	0.00092	2598	8	2474	8	1956	12	2852	16	0.0
5.1	65	105	584	0.18	0.15761	0.00374	2.50576	0.06235	0.14371	0.00148	0.24012	0.00587	2430	28	1274	18	866	8	4350	96	0.0
6.1	210	127	487	0.26	0.20861	0.00228	10.65128	0.09374	0.37030	0.00240	0.10181	0.00078	2556	20	2493	8	2031	11	1960	14	1.2
7.1	68	112	509	0.22	0.08950	0.00214	1.67074	0.03743	0.13539	0.00112	0.04000	0.00036	1415	47	997	14	819	6	793	7	1.5
Mafic dyke 05XF23																					
1	57	436	309	1.41	0.06938	0.00221	1.26337	0.03841	0.13209	0.00150	0.04442	0.00059	910	64	829	17	800	9	879	11	0.0
2	28	271	137	1.99	0.08204	0.00236	1.50710	0.04111	0.13327	0.00148	0.04367	0.00050	1246	55	933	17	807	8	864	10	0.0
3	80	775	399	1.94	0.06954	0.00165	1.28345	0.02857	0.13387	0.00128	0.04385	0.00040	915	48	838	13	810	7	867	8	0.0
4	21	193	107	1.80	0.06793	0.00295	1.25645	0.05271	0.13417	0.00188	0.04428	0.00071	866	88	826	24	812	11	876	14	0.0
5	22	191	113	1.69	0.06963	0.00236	1.26902	0.04119	0.13219	0.00154	0.04413	0.00056	918	68	832	18	800	9	873	11	0.0
6	108	1464	406	3.61	0.06666	0.00159	1.23101	0.02754	0.13395	0.00128	0.04366	0.00032	827	49	815	13	810	7	864	6	0.0
7	20	199	94	2.12	0.07757	0.00263	1.41351	0.04585	0.13216	0.00161	0.04890	0.00058	1136	66	895	19	800	9	965	11	0.0
8	24	212	116	1.83	0.07793	0.00351	1.42541	0.06193	0.13266	0.00201	0.04900	0.00081	1145	87	900	26	803	11	967	16	0.0
9	13	106	65	1.64	0.06805	0.00405	1.24491	0.07189	0.13267	0.00239	0.04600	0.00100	870	119	821	33	803	14	909	19	0.0
10	18	99	78	1.27	0.18561	0.01051	3.39828	0.18207	0.13278	0.00309	0.06700	0.00212	2704	91	1504	42	804	18	1311	40	0.0
11	13	77	75	1.03	0.10571	0.00370	1.94211	0.06452	0.13324	0.00181	0.05169	0.00093	1727	63	1096	22	806	10	1019	18	0.0
12	53	414	300	1.38	0.07169	0.00376	1.31169	0.06657	0.13268	0.00220	0.04376	0.00099	977	103	851	29	803	13	866	19	0.0
13	48	560	220	2.54	0.07125	0.00353	1.31579	0.06296	0.13389	0.00213	0.04395	0.00070	965	98	853	28	810	12	869	14	0.0
14	13	96	69	1.39	0.07470	0.00475	1.37777	0.08500	0.13371	0.00266	0.04951	0.00124	1061	123	880	36	809	15	977	24	0.0
15	55	492	295	1.66	0.07037	0.00195	1.28686	0.03377	0.13257	0.00138	0.03909	0.00044	939	56	840	15	803	8	775	9	0.0
16	21	100	131	0.77	0.06270	0.00677	1.14892	0.12112	0.13284	0.00402	0.05402	0.00270	698	215	777	57	804	23	1063	52	0.0
Mafic dyke 05XF23																					
18	96	1229	406	3.03	0.06749	0.00186	1.24300	0.03242	0.13350	0.00137	0.03949	0.00032	853	56	820	15	808	8	783	6	0.0
19	25	232	120	1.94	0.06668	0.00345	1.22810	0.06159	0.13349	0.00214	0.04608	0.00081	828	104	814	28	808	12	911	16	0.0
20	28	256	139	1.83	0.06871	0.00268	1.27092	0.04771	0.13406	0.00174	0.04445	0.00063	890	79	833	21	811	10	879	12	0.0
21	12	101	67	1.52	0.06411	0.00404	1.18271	0.07246	0.13369	0.00249	0.04088	0.00093	745	128	793	34	809	14	810	18	0.0
22	82	770	428	1.80	0.09199	0.00261	1.70011	0.04558	0.13394	0.00152	0.04276	0.00051	1467	53	1009	17	810	9	846	10	0.0
23	44	367	233	1.58	0.06798	0.00243	1.25404	0.04312	0.13368	0.00163	0.04305	0.00060	868	73	825	19	809	9	852	12	0.0
24	39	398	193	2.06	0.06596	0.00279	1.20669	0.04929	0.13257	0.00181	0.04171	0.00060	805	86	804	23	803	10	826	12	0.0

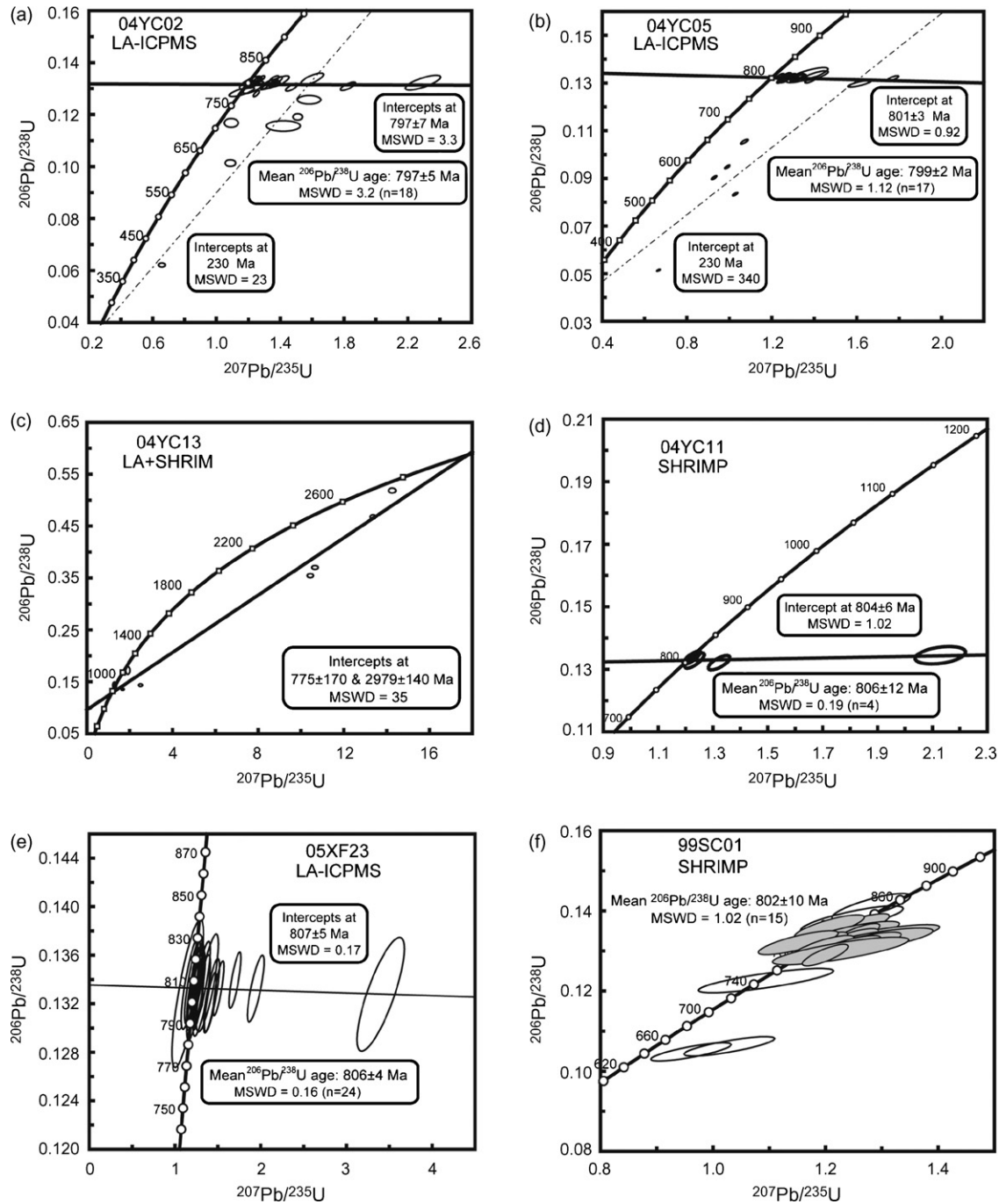


Fig. 10. Zircon U–Pb concordia diagrams for granitoids (a–c) and dykes (d–f) in the Xiaofeng Suite. Data for dyke 99SC1 are after Li et al. (2004b).

stage Hf model ages calculated using a $^{176}\text{Lu}/^{177}\text{Hf}$ ratio of 0.022 yield $T_{\text{DM}2}$ values of 2.7–3.0 Ga, with a weighted mean of 2.9 Ga (Fig. 12c). The data obtained on the core gave an $\varepsilon_{\text{Hf}}(t)$ value of -40.6 if calculated at $t = 800$ Ma, which is too low to be reasonable. If an assumed protolith age of 2.9 Ga is used, a positive $\varepsilon_{\text{Hf}}(t)$ value of 6.4 is obtained. It seems that this core was derived from Mesoarchean juvenile crust.

Twenty-four Lu–Hf isotope analyses were made on zircons from mafic dyke 05XF23. Their $^{176}\text{Hf}/^{177}\text{Hf}$ ratios are 0.281792–0.282103, corresponding to $\varepsilon_{\text{Hf}}(t)$ values of -17.7 to -6.6 at $t = 800$ Ma with a weighted mean of -12.9 (Fig. 11d).

Two-stage Hf model ages are 2.6–3.6 Ga, with a weighted mean of 3.2 Ga (Fig. 12d).

5. Discussion

5.1. Crystallization ages of the Xiaofeng intrusions

A precise constraint on the crystallization ages of the Xiaofeng intrusions is the precondition of interpreting their petrogenesis. A precise dating of mafic magmatic events is important for continental reconstruction. The Huanglingmiao

Table 5
Whole-rock Rb–Sr and Sm–Nd isotopes for intrusive rocks at Xiaofeng in the Huangling Batholith

Sample	Rock type	Rb	Sr	$^{87}\text{Rb}/^{86}\text{Sr}$	$^{87}\text{Sr}/^{86}\text{Sr}$	$^{87}\text{Sr}/^{86}\text{Sr}$	Age (Ma)	$(^{87}\text{Sr}/^{86}\text{Sr})_i$	Sm	Nd	$^{147}\text{Sm}/^{144}\text{Nd}$	$^{143}\text{Nd}/^{144}\text{Nd}$	2S.E.	$\varepsilon_{\text{Nd}}(t)$	T_{DM} (Ga)	T_{DM2} (Ma)
04YC02	Wall-rock granitoid	66.5	335.6	0.571	0.711779	0.705250	800	0.705250	4.41	30.1	0.0884	0.511590	0.000008	−9.3	1.89	2.23
04YC05	Wall-rock granitoid	86.7	227.0	1.102	0.713453	0.700864	800	0.700864	4.24	28.9	0.0887	0.511594	0.000010	−9.2	1.89	2.23
04YC13	Wall-rock granitoid	130.4	73.6	5.126	0.739402	0.680841	800	0.680841	2.01	6.5	0.1863	0.511415	0.000009	−22.8	9.39	3.25
04YC11	dyke	74.6	469.7	0.458	0.711687	0.706455	800	0.706455	4.38	29.4	0.0902	0.511573	0.000009	−9.8	1.94	2.27
04YC20	dyke	53.7	482.0	0.321	0.709473	0.705801	800	0.705801	6.14	35.1	0.1058	0.511829	0.000009	−6.4	1.86	2.00
05XF08	dyke						800		6.27	33.8	0.1121	0.511681	0.000012	−9.9	2.20	2.28
05XF13	Wall-rock granitoid						800		3.60	23.3	0.0935	0.511550	0.000011	−10.6	2.02	2.34
05XF23	dyke						800		6.97	32.6	0.1292	0.511926	0.000013	−6.9	2.20	2.04
05XF24	dyke						800		6.83	33.1	0.1249	0.511923	0.000013	−6.5	2.10	2.00

Suite, which was intruded by the Xiaofeng Suite, was emplaced at 819 ± 7 Ma as dated by the SHRIMP U–Pb technique (Ma et al., 1984). This provides an upper limit for the emplacement ages of the Xiaofeng Suite. The minimum age is constrained at 748 ± 12 Ma by the tuffs in unconformably overlying Liantuo Formation (Ma et al., 1984). Ma et al. (2002) constructed a whole-rock Rb–Sr isochron from five samples of the Xiaofeng Suite, corresponding to an age of 750 ± 57 Ma. Li et al. (2002c) obtained a whole-rock Rb–Sr isochron for a porphyritic granodiorite from the Xiaofeng Suite, yielding an age of 813 ± 85 Ma. This age was interpreted by these authors as the upper limit of the dykes. These Rb–Sr ages have very limited significance because of their large errors. Li et al. (2002c) also reported an ^{40}Ar – ^{39}Ar age of 770 ± 3 Ma for hornblende phenocryst from diabase-porphry veins in the Huangling Batholith.

By means of the SHRIMP U–Pb method, Li et al. (2004b) analyzed 20 zircons from a pale-grey-colored porphyritic dyke ($\text{SiO}_2 = 65.2\%$) at Xiaofeng. Of the 20 grains, three grains suffered Pb loss, two grains gave ages significantly older than the bulk. The remaining 15 analyses gave a weighted mean $^{206}\text{Pb}/^{238}\text{U}$ age of 802 ± 10 Ma (Fig. 10f). On the other hand, Ling et al. (2006) analyzed 31 zircons from a granite in the Xiaofeng Suite, in which most analyses are discordant, only 4 grains are concordant with apparent $^{206}\text{Pb}/^{238}\text{U}$ ages at 327 ± 7 , 871 ± 18 , 737 ± 13 , 764 ± 14 Ma, respectively. A discordia intercept age of 744 ± 22 Ma is only obtained from two analyses. Ling et al. (2006) took the age of 737 ± 13 Ma as its formation age. These diverse results make it necessary to examine the reasonable ages for the Xiaofeng Suite.

We have dated six samples from the Xiaofeng intrusions by the SHRIMP and LA-ICPMS methods. Four of them yield identical U–Pb ages, namely 797 ± 5 Ma for granitoid 04YC02 (Fig. 10a), 799 ± 2 Ma for granitoid 04YC05 (Fig. 10b), 806 ± 12 Ma for felsic dyke 04YC11 (Fig. 10d), and 806 ± 4 Ma for mafic dyke 05XF23 (Fig. 10e). It appears that the granitoids, the felsic and mafic dykes share the same ages of magma crystallization at about 800 Ma. These ages are all derived from the zircons with well-developed concentric zoning or parallel zoning (Fig. 9). A weighted mean of them is 800 ± 3 Ma with $\text{MSWD} = 1.03$. We adopt this age as representing the crystallization age for both granitoids and dykes despite the fact that the dykes were intruded into the granitoids. In this regard, the difference in emplacement time between the dykes and granitoids are within a few million years. This age agrees well with the result of Li et al. (2004b) for a felsic dyke (Fig. 10f), implying that the ages of Ling et al. (2006) are suspicious perhaps because the age distribution is too discrete.

5.2. Relationship between the granitoids and dykes

A characteristic feature of the Xiaofeng intrusions is that they have identical zircon U–Pb ages and similar Hf–Nd–Sr–O isotope compositions. Their relationship must be considered before developing a petrogenetic model.

Although the contents of major and trace elements are different between the dykes and granitoids, good correlations between major and trace elements suggest that they might be cogenetic.

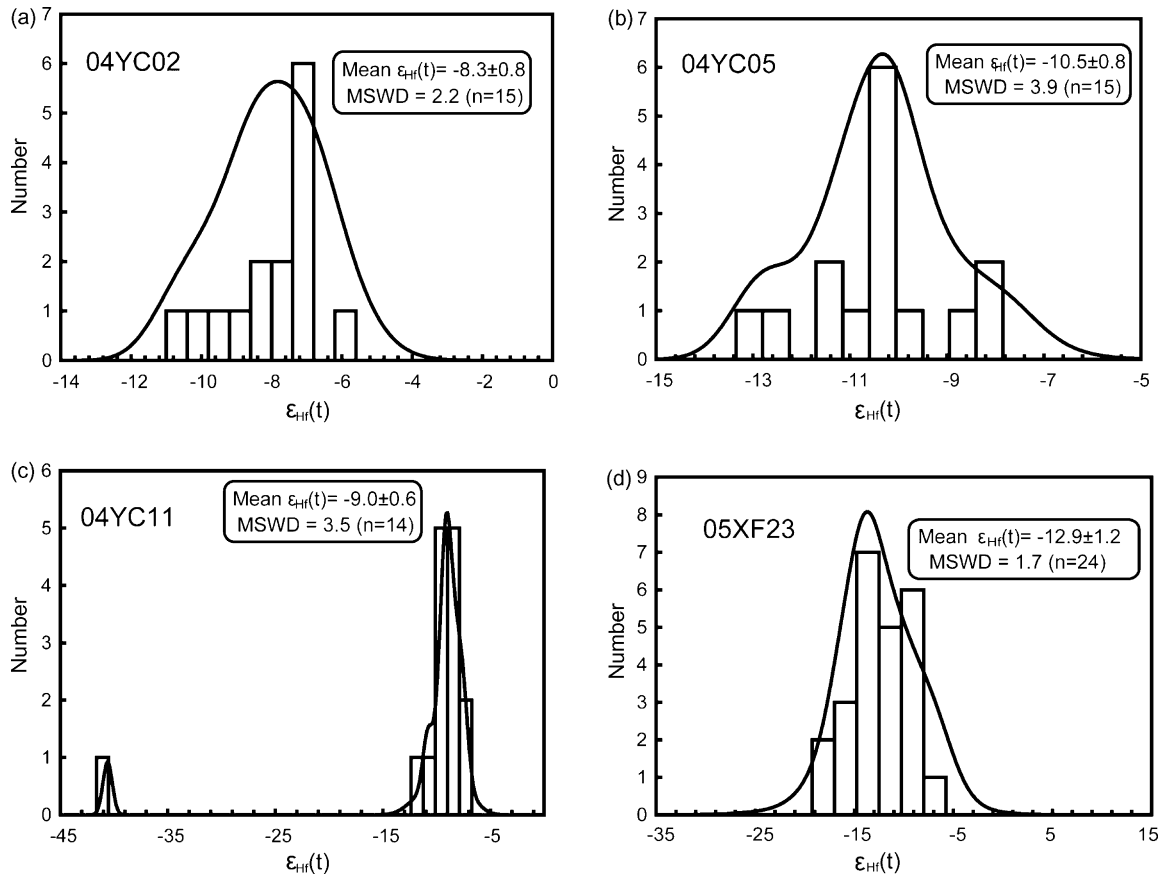


Fig. 11. Statistical distribution of zircon $\epsilon_{\text{Hf}}(t)$ values for granitoids (a and b) and dykes (c and d) in the Xiaofeng Suite.

In the Harker diagram (Fig. 2), both dykes and granitoids fall in the same linear trend for most elements. The REE and trace element distribution patterns for the granitoids and dykes are also very similar (Fig. 6). No complementary relationships exist between the trace element patterns of the mafic and felsic rocks, suggesting that the mafic rocks are neither cumulate nor restite of the felsic rocks.

The mafic dykes have relatively low MgO contents, generally not more than 6% (Table 1). Previous studies indicate that dyke swarms with low MgO are not indicative of high potential temperatures for mantle plumes but decompression melting of ambient mantle (Mayborn and Lesher, 2004). Because the iron contents of primary basaltic magmas increase with increasing depth of melting initiation (Wang et al., 2002), the relatively low iron contents in most mafic dykes at Xiaofeng point to a relatively shallow depth for the initial melting, consistent with the shallow emplacement depth for the granitoids. Thus, both the dykes and granitoids were emplaced in relatively shallow levels.

The mineral O isotopes in the two continuous profiles suggest small-scale high-T water–rock interaction for the granitoids during the intrusion of the dykes (Fig. 8). The availability of surface fluid also implies a shallow depth during the intrusion of the dykes, resulting in the low $\delta^{18}\text{O}$ values of -1.84 to 1.11% for such hydroxyl bearing as biotite, chlorite and epidote. Nevertheless, zircon is a mineral resistant to O isotope exchange with hydrothermal fluid (Zheng and Fu, 1998; Valley, 2003).

Its $\delta^{18}\text{O}$ values of 5.41 – 6.80% for the granitoids indicate that no suprasolidus water–rock interaction occurred during magmatism (Zheng et al., 2004). This is also typical for I-type granite (O’Neil and Chappell, 1977; Chappell, 1999).

Linear correlations can be seen from the plots of $\epsilon_{\text{Nd}}(t)$ versus SiO_2 , MgO, La/Sm and Nd (Fig. 13), which seem to imply mixing between magmas derived from the mantle and the crust, respectively. However, it should be noted that the sample with the most negative $\epsilon_{\text{Nd}}(t)$ value has the lowest Nd content (Fig. 13d), in conflict with the fact that the continental crust has higher Nd than the mantle because of crust–mantle differentiation (Taylor and McLennan, 1995). Thus, magma mixing is not a possible process for petrogenesis of the Xiaofeng intrusions. Neither do the other observations support the magma mixing: (1) the Xiaofeng rocks are bimodal and lack of intermediate rocks with SiO_2 at about 60%, resulting in a discontinuous nature in the Harker diagram (Fig. 2). However, thoroughly mixing is in favor of a continuous rock series; (2) the $\epsilon_{\text{Nd}}(t)$ range of the Xiaofeng rocks is quite narrow, the difference between $\epsilon_{\text{Nd}}(t)$ values for the most felsic and mafic rocks is no greater than 4 (Fig. 13); (3) no mixing texture is observed at the margin between the dykes and granitoids (Fig. 1d), which is more likely to reflect intrusion at quasi-plastic state. Based on these facts, the granitoids and dykes in the Xiaofeng Suite are unlikely to be a rock series of magma mixing. Country-rock contamination is possible, but not a dominant mechanism for these observed linear trends, because the ranges of radiogenic isotope ratios for the

Table 6
Zircon Lu–Hf isotope data for intrusive rocks at Xiaofeng in the Huangling Batholith

No.	Spot	$^{176}\text{Yb}/^{177}\text{Hf}$	$^{176}\text{Lu}/^{177}\text{Hf}$	$^{176}\text{Hf}/^{177}\text{Hf}$	$\pm 2\sigma$	Age (Ma)	$\varepsilon_{\text{Hf}}(t)$	$\pm 2\sigma$	T_{DM1} (Ma)	$\pm 2\sigma$	$f_{\text{Lu/Hf}}$	T_{DM2} (Ma)	$\pm 2\sigma$
Wall-rock granitoid 04YC02													
1	L1.1	0.018025	0.000914	0.282067	0.000025	800	−7.8	0.9	1666	69	−0.97	2762	155
2	L3.1	0.019962	0.001001	0.282095	0.000025	800	−6.8	0.9	1631	69	−0.97	2678	155
3	L2.1	0.021538	0.001083	0.282041	0.000024	800	−8.8	0.9	1710	68	−0.97	2852	153
4	L5.1	0.015386	0.000769	0.282008	0.000023	800	−9.8	0.8	1741	64	−0.98	2939	145
5	L4.1	0.020320	0.001023	0.282011	0.000025	800	−9.8	0.9	1748	69	−0.97	2941	156
6	L6.1	0.019182	0.000983	0.282046	0.000020	800	−8.6	0.7	1698	55	−0.97	2830	125
7	L7.1	0.017414	0.000866	0.281981	0.000022	800	−10.8	0.8	1783	60	−0.97	3029	136
8	L8.1	0.023102	0.001164	0.282050	0.000023	800	−8.5	0.8	1701	64	−0.96	2826	144
9	L14.1	0.017975	0.000893	0.282078	0.000027	800	−7.4	1.0	1650	76	−0.97	2726	173
10	L15.1	0.016076	0.000817	0.282065	0.000028	800	−7.8	1.0	1665	78	−0.98	2764	178
11	L10.1	0.021518	0.001068	0.282093	0.000039	800	−7.0	1.4	1637	109	−0.97	2688	246
12	L9.1	0.026932	0.001325	0.282086	0.000036	800	−7.3	1.3	1657	102	−0.96	2720	228
13	L11.1	0.023228	0.001132	0.282119	0.000029	800	−6.0	1.0	1602	80	−0.97	2607	179
14	L13.1	0.015527	0.000786	0.282087	0.000026	800	−7.0	0.9	1633	71	−0.98	2693	161
15	L12.1	0.023636	0.001171	0.282091	0.000029	800	−7.1	1.0	1644	81	−0.96	2698	182
Wall-rock granitoid 04YC05													
1	L1.1	0.021826	0.001094	0.282066	0.000020	800	−7.9	0.7	1675	55	−0.97	2772	124
2	L2.1	0.020644	0.000998	0.281930	0.000017	800	−12.7	0.6	1860	48	−0.97	3196	109
3	L3.1	0.015638	0.000782	0.281997	0.000019	800	−10.2	0.7	1756	51	−0.98	2974	116
4	L7.1	0.021904	0.001095	0.282038	0.000017	800	−8.9	0.6	1715	48	−0.97	2862	108
5	L5.1	0.027644	0.001307	0.282005	0.000017	800	−10.2	0.6	1770	48	−0.96	2974	108
6	L4.1	0.018488	0.000894	0.282008	0.000018	800	−9.9	0.6	1747	50	−0.97	2946	113
7	L6.1	0.035226	0.001671	0.281990	0.000021	800	−10.9	0.7	1808	58	−0.95	3038	129
8	L8.1	0.028981	0.001305	0.281977	0.000017	800	−11.2	0.6	1809	48	−0.96	3061	109
9	L9.1	0.026110	0.001261	0.281928	0.000018	800	−12.9	0.7	1875	51	−0.96	3212	115
10	L12.1	0.020687	0.001012	0.282062	0.000031	800	−8.0	1.1	1678	88	−0.97	2783	198
11	L10.1	0.025482	0.001195	0.281969	0.000019	800	−11.4	0.7	1815	52	−0.96	3082	116
12	L11.1	0.020945	0.001022	0.281995	0.000022	800	−10.4	0.8	1770	60	−0.97	2992	135
13	L13.1	0.027072	0.001275	0.282000	0.000027	800	−10.4	1.0	1776	74	−0.96	2990	167
14	L14.1	0.022616	0.001110	0.281995	0.000019	800	−10.4	0.7	1774	54	−0.97	2996	121
15	L15.1	0.029100	0.001431	0.282008	0.000017	800	−10.1	0.6	1771	48	−0.96	2970	108
Wall-rock granitoid 04YC13													
1	L1.2	0.021155	0.000952	0.280839	0.000021	2980	−3.2	0.8	3346	58	−0.97	3445	74
2	L1.1	0.023427	0.001016	0.280789	0.000020	2980	−5.1	0.8	3419	54	−0.97	3537	68
3	L3.1	0.011664	0.000632	0.282002	0.000022	800	−9.9	0.8	1743	62	−0.98	2951	141
4	L4.1	0.016374	0.000690	0.281004	0.000043	2980	3.2	1.7	3102	115	−0.98	3136	147
5	L5.1	0.013178	0.000578	0.282024	0.000037	800	−9.1	1.3	1710	101	−0.98	2879	231
6		0.053513	0.002408	0.281969	0.000056	800	−12.0	2.0	1875	160	−0.93	3138	349
Felsic dyke 04YC11													
1	S1.1	0.033026	0.001322	0.281986	0.000012	800	−10.9	0.4	1797	35	−0.96	3035	78
2	S2.1	0.026115	0.000992	0.282081	0.000031	800	−7.3	1.1	1651	87	−0.97	2722	197
3	S3.1	0.021841	0.000919	0.282038	0.000015	800	−8.8	0.5	1706	41	−0.97	2852	93
4	S4.1	0.018266	0.000744	0.282023	0.000013	800	−9.2	0.5	1719	35	−0.98	2891	79
5	Core	0.013654	0.000488	0.281134	0.000012	800	−40.6	0.4	2912	33			
6		0.023148	0.000980	0.281966	0.000034	800	−11.4	1.2	1809	95	−0.97	3080	215
7		0.019780	0.000839	0.282050	0.000019	800	−8.3	0.7	1686	52	−0.97	2810	118
8		0.031775	0.001263	0.282082	0.000013	800	−7.5	0.5	1661	36	−0.96	2732	81
9		0.020695	0.000845	0.282036	0.000014	800	−8.8	0.5	1705	38	−0.97	2854	86
10		0.018869	0.000768	0.282023	0.000015	800	−9.3	0.5	1721	42	−0.98	2894	95
11		0.024283	0.000993	0.282004	0.000016	800	−10.1	0.6	1757	45	−0.97	2963	102
12		0.026409	0.001039	0.282029	0.000016	800	−9.2	0.6	1724	44	−0.97	2885	99
13		0.023124	0.000926	0.282060	0.000015	800	−8.0	0.5	1676	40	−0.97	2784	92
14		0.030893	0.001266	0.282066	0.000017	800	−8.0	0.6	1684	47	−0.96	2782	106
15		0.021348	0.000902	0.282026	0.000014	800	−9.2	0.5	1723	38	−0.97	2890	87
Mafic dyke 05XF23													
1		0.040078	0.001590	0.281864	0.000058	800	−15.3	2.1	1982	163	−0.95	3429	362
2		0.040725	0.001574	0.281928	0.000060	800	−13.1	2.1	1891	169	−0.95	3229	375
3		0.108754	0.004088	0.281924	0.000060	800	−14.5	2.1	2033	181	−0.88	3358	374
4		0.029445	0.001146	0.281977	0.000058	800	−11.1	2.1	1802	161	−0.97	3055	363
5		0.027460	0.001044	0.281938	0.000060	800	−12.4	2.1	1851	166	−0.97	3173	376
6		0.096169	0.003450	0.282072	0.000078	800	−9.0	2.8	1778	232	−0.90	2865	489

Table 6 (Continued)

No.	Spot	$^{176}\text{Yb}/^{177}\text{Hf}$	$^{176}\text{Lu}/^{177}\text{Hf}$	$^{176}\text{Hf}/^{177}\text{Hf}$	$\pm 2\sigma$	Age (Ma)	$\varepsilon_{\text{Hf}}(t)$	$\pm 2\sigma$	T_{DM1} (Ma)	$\pm 2\sigma$	$f_{\text{Lu/Hf}}$	T_{DM2} (Ma)	$\pm 2\sigma$
7		0.032717	0.001239	0.281792	0.000072	800	-17.7	2.6	2064	200	-0.96	3638	449
8		0.041671	0.001584	0.282058	0.000136	800	-8.5	4.8	1709	384	-0.95	2822	854
9		0.021350	0.000821	0.281991	0.000096	800	-10.4	3.4	1767	265	-0.98	2996	602
10		0.027055	0.001154	0.281803	0.000152	800	-17.3	5.4	2044	421	-0.97	3600	948
11		0.026796	0.001064	0.281947	0.000100	800	-12.1	3.5	1840	278	-0.97	3145	626
12		0.047176	0.001680	0.281885	0.000082	800	-14.6	2.9	1957	231	-0.95	3368	512
13		0.068403	0.002608	0.282083	0.000066	800	-8.1	2.3	1721	191	-0.92	2791	414
14		0.019501	0.000725	0.281895	0.000038	800	-13.8	1.3	1895	104	-0.98	3292	238
15		0.050429	0.001966	0.282027	0.000102	800	-9.8	3.6	1771	290	-0.94	2937	639
16		0.024355	0.000869	0.281855	0.000090	800	-15.3	3.2	1957	248	-0.97	3424	562
17		0.034831	0.001326	0.281977	0.000060	800	-11.2	2.1	1811	168	-0.96	3064	376
18		0.110584	0.003976	0.282070	0.000088	800	-9.3	3.1	1808	265	-0.88	2896	551
19		0.027788	0.001095	0.282103	0.000052	800	-6.6	1.8	1624	145	-0.97	2658	327
20		0.033751	0.001279	0.281904	0.000052	800	-13.8	1.8	1910	145	-0.96	3290	325
21		0.025855	0.001045	0.282003	0.000076	800	-10.1	2.7	1761	211	-0.97	2969	477
22		0.091759	0.003442	0.281860	0.000044	800	-16.5	1.6	2091	130	-0.90	3528	274
23		0.037210	0.001534	0.281881	0.000052	800	-14.7	1.8	1955	146	-0.95	3374	325
24		0.046183	0.001806	0.281903	0.000050	800	-14.1	1.8	1939	141	-0.95	3318	312

felsic and mafic rocks are very narrow. After ruling out the possibility of magma mixing and country-rock contamination, the linear trends in Figs. 2 and 13 can only be interpreted by their composition-correlated sources.

The Nd–Hf isotope compositions of the granitoids and dykes are both extremely enriched. Zircon $\varepsilon_{\text{Hf}}(t)$ values are plotted in Fig. 14 to compare with their whole-rock $\varepsilon_{\text{Nd}}(t)$ values. It is noted that they have similar ranges and all fall into the area defined

by the terrestrial array (Vervoort et al., 1999). Four samples of the granitoid were analyzed for their whole-rock Nd isotopes. Except for one sample (04YC13), their $\varepsilon_{\text{Nd}}(t)$ values are -9.2 to -10.6 . The single-stage Nd model ages are 1.85–2.02 Ga and two-stage Nd model ages are 2.2–2.3 Ga. Zircon Hf isotope analyses for the three of the four granitoids yield similarly monomodal distribution patterns. The $\varepsilon_{\text{Hf}}(t)$ values are -10.5 to -8.3 (Fig. 11), corresponding to two-stage Hf model ages of

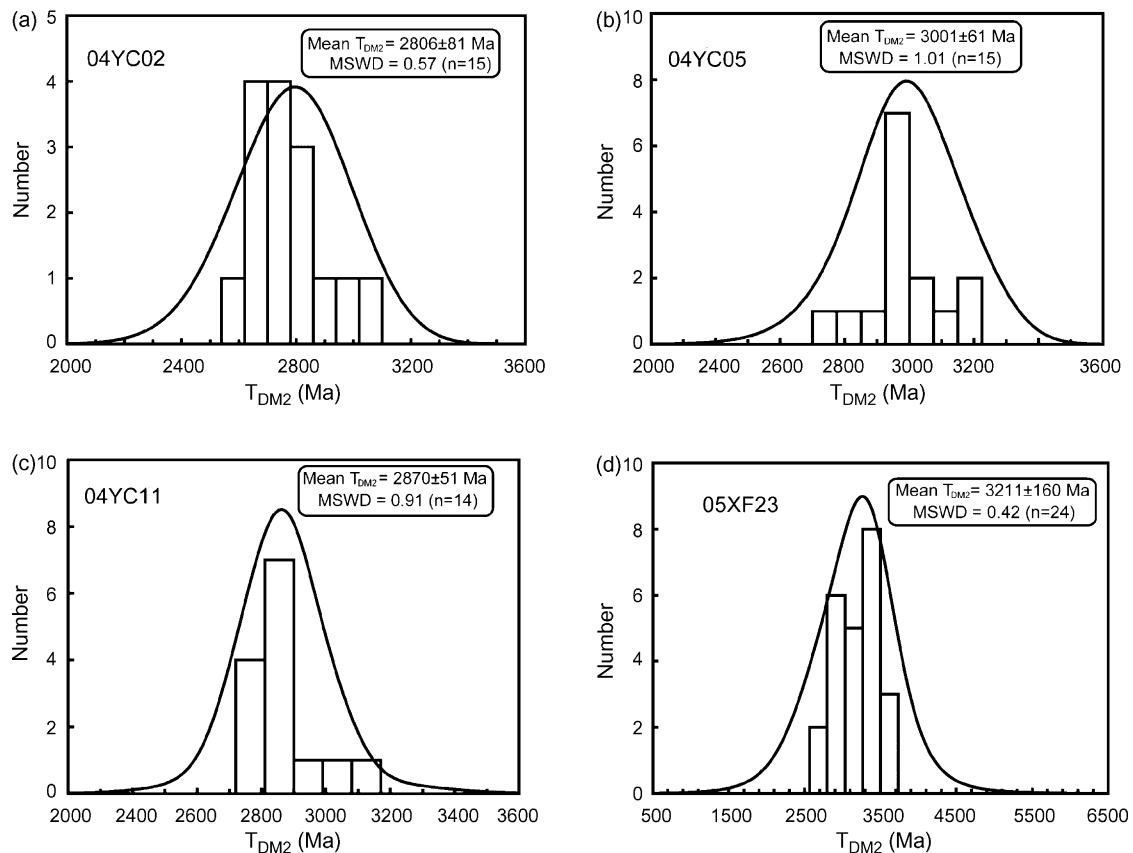


Fig. 12. Statistical distribution of zircon Hf model ages for granitoids (a and b) and dykes (c and d) in the Xiaofeng Suite.

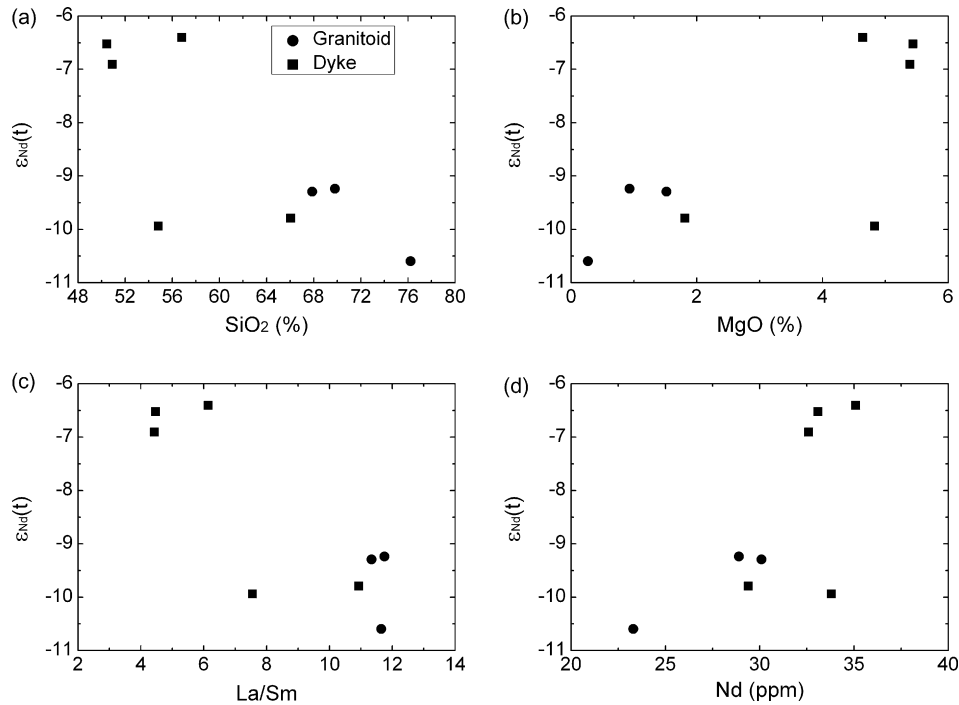


Fig. 13. Plots of $\epsilon_{Nd}(t)$ vs. SiO_2 , MgO , La/Sm and Nd for Neoproterozoic granitoids and dykes in the Xiaofeng Suite.

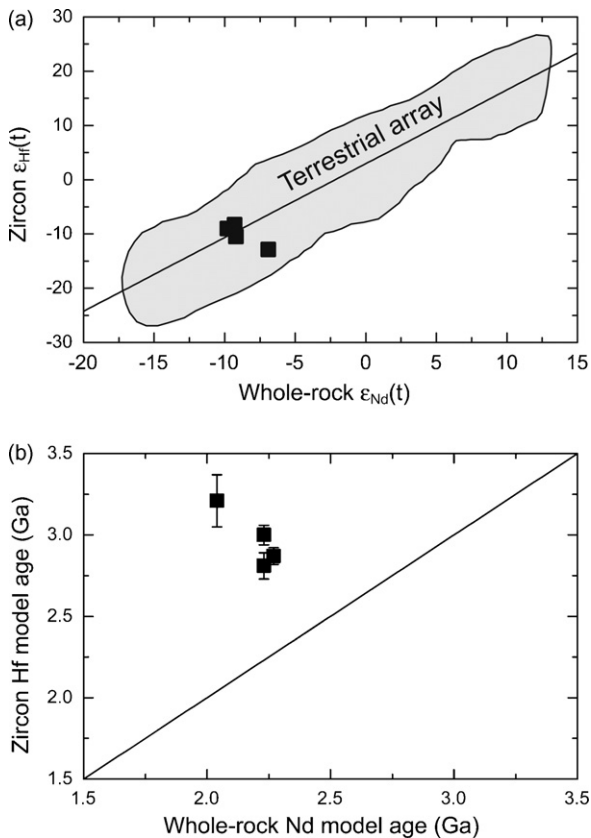


Fig. 14. The relationships between zircon Hf and whole-rock Nd isotopes in Neoproterozoic igneous rocks at Xiaofeng. (a) $\epsilon_{Hf}(t)$ values vs. whole-rock $\epsilon_{Nd}(t)$ values, with terrestrial array after Vervoort et al. (1999). (b) Zircon Hf model ages vs. whole-rock Nd model ages.

2.8–3.0 Ga (Fig. 12). Five samples of the mafic to felsic dykes (SiO_2 contents are from 50.44 to 66.05%) were analyzed for their Nd isotopes, yielding $\epsilon_{Nd}(t)$ values of -9.9 to -6.4 . Correspondingly, their single-stage Nd model ages are 1.9–2.2 Ga and two-stage Nd model ages are 2.0–2.3 Ga. The mafic and felsic dykes have the similar $\epsilon_{Nd}(t)$ values, suggesting their derivation from the same source of continental lithosphere. The negative $\epsilon_{Nd}(t)$ values for the dykes preclude the depleted asthenosphere mantle as a possible source. Zircon Hf isotope analyses were conducted for a felsic and a mafic dykes. For the felsic dyke, the $\epsilon_{Hf}(t)$ values have a weighted mean of -9.0 (Fig. 11c) except an extremely negative $\epsilon_{Hf}(t)$ value on a core. The corresponding two-stage Hf model ages are about 2.9 Ga (Fig. 12c) similar to those for the granitoids, suggesting that they have the similar nature of source rocks. For the mafic dyke, 24 $\epsilon_{Hf}(t)$ values yield a weighted mean of -12.9 (Fig. 11d) and two-stage Hf model ages of 2.6–3.6 Ga with a weighted mean of 3.2 Ga (Fig. 12d). The two-stage Nd model ages are significantly younger than the Hf model ages. This can be well explained by the zircon effect because whole-rock Sm–Nd isotopes are susceptible to elements Sm/Nd differentiation during partial melting (Patchett et al., 1984; Wu et al., 2006a; Zheng et al., 2007). Because radiogenic Hf isotopes in igneous zircon are capable of surviving partial melting, zircon Hf model ages can provide a more reasonable proxy for the age of source rocks (Kemp et al., 2006; Nebel et al., 2007). In this regard, reasonable determination of Sm/Nd and Lu/Hf isotope ratios for source rocks is critical to reconcile the Hf–Nd decoupling in the two-stage evolution model.

The Archean Hf model ages for the Xiaofeng intrusions suggest a link between their origins and the Kongling Complex, the only Archean continental nucleus outcropped in the Yangtze Block. Zircon U–Pb dating on these rocks reveal an important

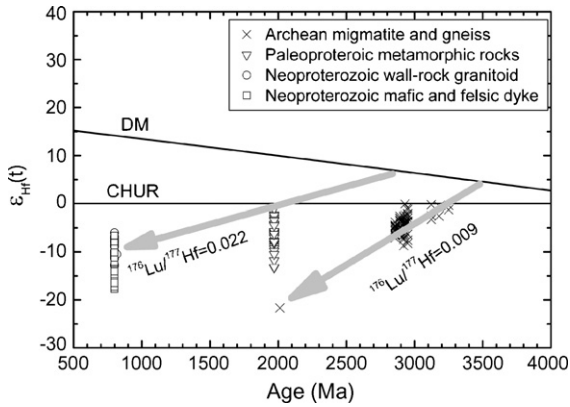


Fig. 15. Plot of zircon $\epsilon_{\text{Hf}}(t)$ values vs. U–Pb ages for Neoproterozoic granitoids and dykes in the Xiaofeng Suite. Also shown are data for Archean and Paleoproterozoic rocks (after Zhang et al., 2006a,b; Zheng et al., 2006b). The evolution line of depleted mantle is constrained by a present-day $^{176}\text{Lu}/^{177}\text{Hf}$ ratio of 0.28325 (Nowell et al., 1998) and $^{176}\text{Lu}/^{177}\text{Hf}$ ratio of 0.0384 (Griffin et al., 2000).

magmatic activity at 2.9–3.0 Ga (Qiu et al., 2000; Zhang et al., 2006a), although the growth of continental crust had begun much earlier (Zhang et al., 2006c). The consistency exists between the zircon Hf model ages and the major U–Pb ages for magmatism in the Kongling Complex, implying that the source rocks of the Xiaofeng intrusions are Archean continental crust. Although the zircon Hf model ages for both granitoids and dykes are not “real” ages, their consistency with the zircon U–Pb ages for the Kongling Complex implies contemporaneous formation of their source rocks with the Kongling Complex. In other words, the source of the granitoids and dykes are the Archean continental crust.

Candidates for the source rocks of the mafic dykes can be the continental lower crust or subcontinental lithospheric mantle. Both of them are a part of cratonic lithosphere formed in the Archean. Considering the continent-like REE and trace element patterns for the mafic dykes, we prefer the lower crust as their source, although this requires relatively high degree of partial melting. In Fig. 15, we plot zircon $\epsilon_{\text{Hf}}(t)$ values for the Xiaofeng intrusions together with those for the Kongling Complex, including Archean migmatite and gneiss, Paleoproterozoic metamorphic rocks (Zhang et al., 2006a,b; Zheng et al., 2006b). The source rocks of the Neoproterozoic igneous rocks at Xiaofeng were extracted from the depleted mantle at about 2.9 Ga. This suggests that the 2.9 Ga magmatism in the Yangtze Block is associated with growth of juvenile crust, although this event is not recorded in the Kongling rocks. Thus, the granitoids and dykes formed in the same event at similar depths, by anatexis of the different parts of continental lithosphere in the Mesoarchean ages.

6. Constraints on petrogenesis of the Xiaofeng intrusions

Bearing the above conclusions in mind, let us consider a petrogenetic model for the Xiaofeng intrusions. Any interpretation concerning their petrogenesis must be consistent with the

observations listed before. As mentioned in the introduction, the three types of model have been proposed for the petrogenesis of Neoproterozoic igneous rocks in South China. Although they are based on different views of observations and interpretations, growth and reworking of juvenile and ancient crusts are central to resolution of the debates. Geochemically, contemporaneous growth of juvenile crust is required for both plume- and arc-derived rocks. In view of trace elements, particularly, the plume-derived rocks are commonly associated with OIB-like pattern with enrichment of high field strength elements (HFSE), whereas arc-sourced rocks are characterized by their extreme depletion of HFSE but significant enrichment of large ion lithospheric element (LILE) and light rare earth element (LREE).

When continental crust thickens during collisional orogeny, on the other hand, gravitational instability may trigger extensional collapse (or orogenic collapse) above a normal-sense shear zone (or orogenic detachment). Extensional collapse has been linked to the emplacement of post-collisional granites and to the growth of post-collisional sedimentary basins in the interior of orogens (Dewey, 1977; Malavieille et al., 1990; Liu and Shen, 1998; Rey et al., 2001). This process is closely associated with a thermal impact on orogenic roots in response to lithospheric extension due to plate reorganization, without envisaging of material contributions from mantle plume or island arc (Zheng et al., 2007). It has been used to account for initiation of post-collisional magmatism at mid-Neoproterozoic (830–820 Ma) following arc-continent collision at about 900 ± 20 Ma in the Jiangnan Orogen (Wu et al., 2006a; Zheng et al., 2007), and at early Cretaceous subsequent to continent-continent collision at Triassic in the Dabie-Sulu orogenic belt (Xie et al., 2006).

Because the involvement of juvenile crust is a central issue to test the three models of petrogenesis, we list below some coeval mafic rocks with ages at about 800 Ma, including basalts, dykes, gabbroic intrusions along the Kangdian Rift in the western margin of the Yangtze Block. Alkaline basalts from bimodal volcanic rocks at Suxiong have a zircon U–Pb age of 803 ± 12 Ma and whole-rock $\epsilon_{\text{Nd}}(t)$ values of 5–6 and $\epsilon_{\text{Hf}}(t)$ values of 4.3–8.0, high Fe/Mn ratios of 41.9–97.6, pronounced enrichment in Th, Ta, Nb, LREE, Sr, P, Zr, Hf, Ti, smooth LREE-enriched patterns and generally ‘humped’ trace element spidergrams (Li et al., 2002b, 2005). Some of them have the OIB-like trace element pattern. Gabbro at Lengqi has a zircon U–Pb age of 808 ± 12 Ma and a whole-rock $\epsilon_{\text{Nd}}(t)$ value of 3.6–4.4 (Li et al., 2002b). Two groups of mafic dykes in the Luding-Shimian area show zircon U–Pb ages of 779 ± 6 and 758 ± 37 Ma, whole-rock $\epsilon_{\text{Nd}}(t)$ values of 1.73–8.62 and $\epsilon_{\text{Hf}}(t)$ values of 7.86–17.44 (Lin et al., 2007). Basalt in the Tiechuanshan Formation has a zircon U–Pb age of 817 ± 5 Ma and whole-rock $\epsilon_{\text{Nd}}(t)$ values of 4.6–5.3 for tholeiitic basalts and 0.2–3.8 for alkaline basalts (Ling et al., 2003). Gabbro at Wangjiangshan in the northwestern margin of the Yangtze Block exhibits a zircon U–Pb age of 819 ± 10 Ma and whole-rock $\epsilon_{\text{Nd}}(t)$ values of 3.5–5.9 (Zhou et al., 2002a). Similar positive $\epsilon_{\text{Hf}}(t)$ values were observed for zircons from mid-Neoproterozoic igneous rocks elsewhere in the Yangtze Block, including granodiorite at its southeastern margin (Wu et al., 2006a), bimodal intrusions in its northern margin (Zheng

et al., 2006a; Chen et al., 2007b) and western margin (Zheng et al., 2007).

For the initial Hf isotope compositions cited above, most of the positive $\varepsilon_{\text{Hf}}(t)$ values are still lower than those for the coeval depleted mantle and give Hf model ages of late Mesoproterozoic. Only a few of the positive $\varepsilon_{\text{Nd}}(t)$ and $\varepsilon_{\text{Hf}}(t)$ values approach those for the coeval depleted mantle, yielding the Hf model ages of early Neoproterozoic. Thus, reworking of late Mesoproterozoic juvenile crust is predominated for petrogenesis of many mid-Neoproterozoic igneous rocks (Zheng et al., 2007), leaving only sporadic occurrences of mid-Neoproterozoic juvenile crust in the northern margin of the Yangtze Block (Zheng et al., 2006a). In either case, the mid-Neoproterozoic reworking of juvenile crust occurred in the rift tectonic zones that were developed along the early Neoproterozoic arc-continent collision orogens (Wu et al., 2006a; Zheng et al., 2006a, 2007; Chen et al., 2007b). For the Xiaofeng intrusions, however, they are characterized by the extremely negative $\varepsilon_{\text{Hf}}(t)$ and $\varepsilon_{\text{Nd}}(t)$ values (Fig. 11), corresponding to reworking of ancient Archean lithosphere (Fig. 12).

Another important difference between the Xiaofeng intrusions and the other mid-Neoproterozoic rocks in the periphery of the Yangtze Block is their regional tectonic setting and evolution history. The only and oldest continental nucleus of the Yangtze Block, the Kongling Complex, lies in the Huangling area (Fig. 1). It is separated into two parts by the Huangling Batholith. Part of the Kongling Complex, mainly gneissic granites, even extended to the Xiaofeng area and occurred as the country rock for the Xiaofeng intrusions. Previous studies have demonstrated that the growth of Kongling crust occurred since the Paleoproterozoic in this area (Zhang et al., 2006a,c) and experienced reworking in the mid-Paleoproterozoic (Zhang et al., 2006b). This mid-Paleoproterozoic metamorphism provides a connection between the Yangtze Block and the global tectonomagmatism in the Paleoproterozoic, marking arc-continent collision during assembly of the supercontinent Columbia (Zhang et al., 2006b). In the mid-Neoproterozoic, a combination of the gravitational instability and the lithospheric extension results in tectonic collapse of the collision orogen and thus the eventual anatexis of Archean lithosphere at about 800 Ma. This episode of magmatism is a tectonothermal response to lithospheric extension prior to breakup of the supercontinent Rodinia. Rifting of South China from Rodinia appears to occur along its northern margin at about 750 Ma (Zheng et al., 2006a).

The plume-rift model of Li et al. (2003a,b) cannot explain the following observations: (1) plume-derived magmatism is related to the growth of juvenile crust. However, no signature of mid-Neoproterozoic juvenile crust is found in the Xiaofeng intrusions; (2) mafic rocks derived from melting of mantle plume have OIB-like trace element patterns. However, the trace elements in the Xiaofeng mafic dykes are characterized by depletion of Nb and Ta but enrichment of LILE (Fig. 6), typical of differentiated continental crust; (3) mafic rocks related to the mantle plume have high MgO contents. However, the highest MgO content of the mafic dykes at Xiaofeng is only 5.44% (Table 1). In view of these arguments, a plume-rift origin for the Xiaofeng Suite is declined.

The island-arc model of Zhou et al. (2002a,b) is also incompatible with our observations. (1) Arc accretion to continent would generally form a linear belt along the convergent continental margin. However, the Xiaofeng intrusions are located in the interior of the Yangtze Block, about 300 km to the south of the Qinling orogen. (2) If the Grenvillian subduction of oceanic crust beneath the Yangtze Block would bring about arc magmatism along its periphery, contemporaneous growth of juvenile crust is certainly associated with its igneous product. This has been exemplified for Neoproterozoic S-type granodiorite in the eastern part of the Jiangnan Orogen (Wu et al., 2006a). However, extremely negative $\varepsilon_{\text{Nd}}(t)$ and $\varepsilon_{\text{Hf}}(t)$ values as well as the zircon Hf model ages of 2.8–3.2 Ga for the Xiaofeng intrusions indicate that their source rocks are the Mesoproterozoic ancient crust. Thus, it cannot be the juvenile crust of late Mesoproterozoic. (3) Even if the continental arc would serve as the source rocks of the Xiaofeng intrusions, it cannot be a Paleoproterozoic one as recognized for Neoproterozoic S-type granites in the southern part of the Jiangnan Orogen (Zheng et al., 2007). Since the distribution patterns of REE and trace elements in the Xiaofeng intrusions look like arc-derived materials, the Mesoproterozoic ancient arc could be involved by continental accretion during the Neoproterozoic in South China. Thus, a slab-arc origin for the Xiaofeng intrusions is ruled out by the geochemical results.

As addressed by Zheng et al. (2007) in the plate-rift model, understanding the petrogenesis of Neoproterozoic igneous rocks in South China is essential for assessing the geodynamics of supercontinental rifting along preexisting arc-continent collision orogens. The periphery of the Yangtze Block is an outstanding example of such orogens. Its northern margin was developed into volcanic rifted margins in the mid-Neoproterozoic (Zheng et al., 2006a; Chen et al., 2007b), with extensively fossil geothermal systems in the syn-rift stage (780–740 Ma). This is associated with high heat flow and high-T water–rock interaction, remelting of hydrothermal altered rocks and local low $\delta^{18}\text{O}$ magmatism, and fast accumulation of physically weathered sediments in rift tectonic zones (Zheng et al., 2004, 2006a; Chen et al., 2007b; Tang et al., 2008; Wu et al., 2007). In contrast, the Jiangnan Orogen is the early Neoproterozoic arc-continent collision orogen along the southeastern margin of the Yangtze Block. It suffered pre-rift tectonic collapse to form S-type granodiorite and granite at about 825 Ma (Wu et al., 2006a; Zheng et al., 2007), but it did not broken up during the rifting of South China from Rodinia at about 750 Ma. In either case, tectonic collapse and subsequent rifting occurred in the periphery of the Yangtze Block to result in the pre-rift and syn-rift magmatism. Its source materials involve not only the juvenile crust of late Mesoproterozoic to early Neoproterozoic ages, but also the ancient crust of middle Paleoproterozoic ages.

Much progress has been made in the past few years on Neoproterozoic igneous petrogenesis within the framework of the tectonic evolution from supercontinental rift to breakup in South China. Major geodynamic stages associated with supercontinental rifting in the periphery of the Yangtze Block can be outlined from a series of studies concerning the plate-rift model (Wu et al., 2006a; Zheng et al., 2006a, 2007; Tang et al., 2008): (1) the Grenvillian subduction of oceanic crust to cause

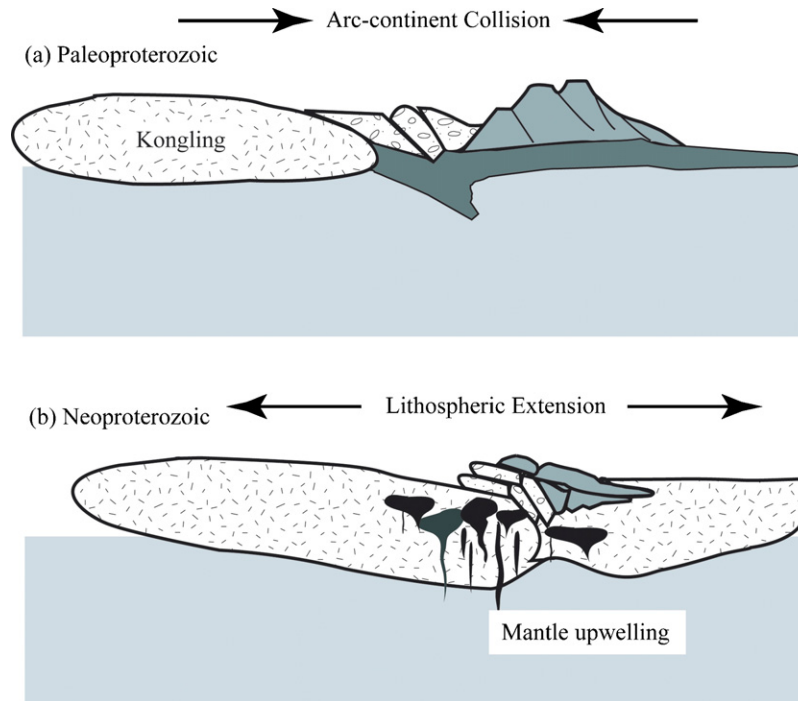


Fig. 16. A schematic model for petrogenesis of Neoproterozoic dykes and wall-rock granitoids in the Xiaofeng Suite.

oceanic and continental arc magmatism in about 1.3–1.0 Ga; (2) arc-continent collision and continental accretion, metamorphism and syn-collisional magmatism at about 900 ± 20 Ma; (3) tectonic collapse of collision orogens and post-collisional magmatism at about 830–800 Ma, without occurrence of contemporaneous mantle plume or arc magmatism; (4) extensive syn-rift magmatism at about 780–740 Ma in response to the tectonic advance from supercontinental rift to breakup. During this period, the new plate boundary was reorganized from a transtensional deformation zone into en-echelon pull-apart basins that were separated by transform fault systems; maturation of these pull-apart basins into the new spreading centers, leading to the breakup of South China from Rodinia.

In the light of the above arguments, a plausible model for petrogenesis of the Xiaofeng intrusions is the tectonic collapse of thickened intracontinental orogen (Fig. 16). This intracontinental orogen formed by the arc-continent collision in the mid-Paleoproterozoic (Zhang et al., 2006b) or earlier. Because arc-continent collision is a basic mechanism for continental accretion (Rudnick, 1995; Taylor and McLennan, 1995), for the Xiaofeng case it would occur surrounding the Archean Kongling Complex (microcontinent). In any case, the collision-thickened orogen is composed of ancient Archean continental lithosphere and it has nothing to do with the Grenvillian subduction of oceanic crust. Collisional orogens are gravitationally unstable and thus tend to collapse in response to the lithospheric extension. This has dual effects on anatexis: (1) heating of orogenic lithospheric root due to gravitational collapse, and (2) asthenospheric upwelling due to lithospheric thinning, providing heat for anatexis. Although collapsed orogens are not a preferred site of developing supercontinental rifting into breakup, a transformation of tectonic framework from compressional

to extensional regimes would take place at about 800 Ma in South China. The orogenic collapse can lead to heating of the lithospheric keel and thus its anatexis at appropriate depths. Contemporaneous melting of different materials at different depths results in the quasi-bimodal magmatism at Xiaofeng (Fig. 16b).

In summary, the igneous rocks of the Xiaofeng Suite are derived from anatexis of Archean precursors at the mid-Neoproterozoic. Possible source rocks of the granitoids and dykes are the Archean continental crust (perhaps including underlying subcontinental lithosphere mantle). The bulk process represents a typical intra-lithosphere differentiation of geochemistry, without any addition of asthenospheric mantle. It is the differentiation that leads to the compositional evolution of continental lithosphere. Although the growth of juvenile crust via underplating of asthenospheric mantle can provide significant heat for the reworking of continental lithosphere, it is not so for the Xiaofeng intrusions because no juvenile crust has been identified in them. In other words, the compositional evolution of continental lithosphere at about 800 Ma in the Yangtze Gorge was not accompanied by extraction of juvenile crust from the depleted mantle. No active continental margin or mantle plume occurred in this region at that time. Thus, the petrogenesis of the Xiaofeng intrusions lends support to the plate-rift model.

7. Conclusions

Zircon U–Pb dating on mafic-felsic compound dykes and wall-rock granitoids in the Xiaofeng Suite demonstrates their contemporaneous crystallization at 800 ± 3 Ma. The same nature of geochemical reservoirs for their magma sources is evident from the compositions of whole-rock elements and

Sr–Nd–O isotopes as well as zircon Hf isotopes. Zircon O isotopes are typical for I-type granite. Both zircon $\varepsilon_{\text{Hf}}(t)$ and whole-rock $\varepsilon_{\text{Nd}}(t)$ values are extremely negative, corresponding to reworking of ancient Archean rather than juvenile Neoproterozoic crust. Zircon Hf model ages are very similar to each other, all from 2.8 to 3.2 Ga, suggesting that they are derived from anatexis of Mesoarchean lithosphere. Mineral O isotopes suggest small-scale high-T water–rock interaction during the intrusion of the Xiaofeng dykes into the wall-rock granitoids.

The involvement of juvenile crust is not identified in the Xiaofeng intrusions. No active continental margin occurred during the early Neoproterozoic in the Yangtze Gorge. Thus, neither mantle superplume nor oceanic arc is responsible for their origin. Instead, the plate-rift model has interpreted all the observations available from the mid-Neoproterozoic igneous rocks. Therefore, a plausible model for their petrogenesis is the tectonic collapse of thickened intracontinental orogen due to lithospheric extension in response to plate reorganization prior to the Rodinia breakup. This episode of Neoproterozoic igneous rocks in South China result from the early phase of plate-rift magmatism, with contrasting contributions in the source nature: the ancient lithosphere of Mesoarchean ages in the Yangtze Gorge, but the juvenile crust of early Neoproterozoic to late Mesoproterozoic ages along the southeastern, northern, and western margins of the Yangtze Block.

Acknowledgments

This study was supported by the Chinese Academy of Sciences (kzcx2-yw-131) and the Natural Science Foundation of China (40334036). Thanks are due to Yuruo Shi for his assistance with SHRIMP U–Pb dating, to Xiaoming Liu for his assistance with LA-ICPMS U–Pb dating, and to Liewen Xie and Yueheng Yang for their assistance with LA-MC-ICPMS Lu–Hf isotope analysis. Comments by Min Sun and Xiaolei Wang help improvement of the presentation.

References

- Amelin, Y., Lee, D.C., Halliday, A.N., 2000. Early-middle Archaean crustal evolution deduced from Lu–Hf and U–Pb isotopic studies of single zircon grains. *Geochim. Cosmochim. Acta* 64, 4205–4225.
- Ames, L., Zhou, G.Z., Xiong, B.C., 1996. Geochronology and isotopic character of ultrahigh-pressure metamorphism with implications for collision of the Sino-Korean and Yangtze cratons, central China. *Tectonics* 15, 472–489.
- Andersen, T., 2002. Correction of common lead in U–Pb analyses that do not report Pb-204. *Chem. Geol.* 192, 59–79.
- Blichert-Toft, J., Albarede, F., 1997. The Lu–Hf isotope geochemistry of chondrites and the evolution of the mantle-crust system. *Earth Planet. Sci. Lett.* 148, 243–258.
- Chappell, B.W., 1999. Aluminium saturation in I- and S-type granites and the characterization of fractionated haplogranites. *Lithos* 46, 535–551.
- Chappell, B.W., White, A.J.R., Williams, I.S., Wyborn, D., 2004. Low- and high-temperature granites. *Trans. R. Soc. Edinburgh: Earth Sci.* 95, 125–140.
- Chen, F.K., Guo, J.H., Jiang, L.L., Siebel, W., Cong, B.L., Satir, M., 2003. Provenance of the Beihuaiyang lower-grade metamorphic zone of the Dabie ultrahigh-pressure collisional orogen, China: evidence from zircon ages. *J. Asian Earth Sci.* 22, 343–352.
- Chen, J.F., Zheng, Y.-F., Zhao, Z.-F., Li, B., Xie, Z., Gong, B., Qian, H., 2007a. Relationships between O isotope equilibrium, mineral alteration and Rb–Sr chronometric validity in granitoids: implications for determination of cooling rate. *Contrib. Mineral. Petrol.* 153, 251–271.
- Chen, R.-X., Zheng, Y.-F., Zhao, Z.-F., Tang, J., Wu, F.-Y., Liu, X.-M., 2007b. Zircon U–Pb ages and Hf isotopes in ultrahigh-pressure metamorphic rocks from the Chinese Continental Scientific Drilling project. *J. Metamorph. Geol.* 25, 873–894.
- Compston, W., Williams, I.S., Kirschvink, J.L., Zhang, Z.C., Ma, G.G., 1992. Zircon U–Pb ages for the Early Cambrian time-scale. *J. Geol. Soc. London* 149, 171–184.
- Defant, M.J., Drummond, M.S., 1990. Derivation of some modern arc magmas by melting of young subducted lithosphere. *Nature* 347, 662–665.
- Dewey, J.F., 1977. Extensional collapse of orogens. *Tectonics* 7, 1123–1139.
- Giletti, B.J., 1986. Diffusion effects on oxygen isotope temperatures of slowly cooled igneous and metamorphic rocks. *Earth Planet. Sci. Lett.* 77, 218–228.
- Gong, B., Zheng, Y.-F., Chen, R.-X., 2007. TC/EA-MS online determination of hydrogen isotope composition and water concentration in eclogitic garnet. *Phys. Chem. Miner.* 34, 687–698.
- Griffin, W.L., Pearson, N.J., Belousova, E., Jackson, S.E., van Achterbergh, E., O'Reilly, S.Y., Shee, S.R., 2000. The Hf isotope composition of cratonic mantle: LAM-MC-ICPMS analysis of zircon megacrysts in kimberlites. *Geochim. Cosmochim. Acta* 64, 133–147.
- Hacker, B.R., Ratschbacher, L., Webb, L., McWilliams, M., Ireland, T., Calvert, A., Dong, S., Wenk, H.R., 2000. Exhumation of ultrahigh-pressure continental crust in east central China: Late Triassic–Early Jurassic tectonic unroofing. *J. Geophys. Res.* 105, 13339–13364.
- Hawkesworth, C.J., Kemp, A.I.S., 2006. Evolution of the continental crust. *Nature* 443, 811–817.
- Huang, J., Zheng, Y.-F., Zhao, Z.-F., et al., 2006. Melting of subducted continent: element and isotopic evidence for a genetic relationship between Neoproterozoic and Mesozoic granitoids in the Sulu orogen. *Chem. Geol.* 229, 227–256.
- Jahn, B.-m., Condie, K.C., 1995. Evolution of the Kaapvaal-Craton as viewed from geochemical and Sm–Nd isotopic analyses of intracratonic pelites. *Geochim. Cosmochim. Acta* 59, 2239–2258.
- Kelemen, P.B., Hanghoj, K., Greene, A.R., 2003. One view of the Geochemistry of subduction-related magmatic arcs, with an emphasis on primitive andesite and lower crust. *Treatise Geochem.* 3, 593–660.
- Kemp, A.I.S., Hawkesworth, C.J., Paterson, B.A., Kinny, P.D., 2006. Episodic growth of the Gondwana supercontinent from hafnium and oxygen isotopes in zircon. *Nature* 439, 580–583.
- Lee, C.-Y., Tsai, J.-H., Ho, H.-H., Yang, T.F., Chung, S.-L., Chen, C.-H., 1997. Quantitative analysis in rock samples by an X-ray fluorescence spectrometer. I. Major elements. In: Abstract Volume for Annual Meeting of the Geological Society of China, pp. 418–420 (in Chinese).
- Li, Z.X., Li, X.H., Kinny, P.D., Wang, J., 1999. The breakup of Rodinia: did it start with a mantle plume beneath South China? *Earth Planet. Sci. Lett.* 173, 171–181.
- Li, X.H., Li, Z.X., Zhou, H.W., Liu, Y., Kinny, P.D., 2002a. U–Pb zircon geochronology, geochemistry and Nd isotopic study of Neoproterozoic bimodal volcanic rocks in the Kangdian Rift of South China: implications for the initial rifting of Rodinia. *Precambrian Res.* 113, 135–154.
- Li, X.H., Li, Z.-X., Zhou, H., Liu, Y., Liang, X., 2002b. U–Pb zircon geochronological, geochemical and Nd isotopic study of Neoproterozoic basaltic magmatism in western Sichuan: petrogenesis and geodynamic implications. *Earth Sci. Front.* 9, 329–338 (in Chinese with English abstract).
- Li, Z., Wang, G., Zhang, Z., 2002c. Isotopic age spectrum of the Huangling granitic batholith, western Hubei. *Geol. Miner. Res. South China* 3 (3), 19–28 (in Chinese with English abstract).
- Li, Z.X., Li, X.H., Kinny, P.D., Wang, J., Zhang, S., Zhou, H., 2003a. Geochronology of Neoproterozoic syn-rift magmatism in the Yangtze Craton, South China and correlations with other continents: evidence for a mantle superplume that broke up Rodinia. *Precambrian Res.* 122, 85–109.
- Li, X.H., Li, Z.X., Ge, W.C., Zhou, H.W., Li, W.X., Liu, Y., Wingate, M.T.D., 2003b. Neoproterozoic granitoids in South China: crustal melting above a mantle plume at ca. 825 Ma? *Precambrian Res.* 122, 45–83.
- Li, X.-H., Li, Z.-X., Ge, W.C., Zhou, H.W., Li, W.X., Liu, Y., Wingate, M.T.D., 2004a. Reply to the comment: Mantle plume-, but not arc-related Neoproterozoic magmatism in South China. *Precambrian Res.* 132, 405–407.

- Li, Z.X., Evans, D.A.D., Zhang, S., 2004b. A 90° spin on Rodinia: possible causal links between the Neoproterozoic supercontinent, superplume, true polar wander and low-latitude glaciation. *Earth Planet. Sci. Lett.* 220, 409–421.
- Li, X.H., Qi, C.S., Liu, Y., Liang, X.R., Tu, X.L., Xie, L.W., Yang, Y.H., 2005. Petrogenesis of the Neoproterozoic bimodal volcanic rocks along the western margin of the Yangtze Block: new constraints from Hf isotopes and Fe/Mn ratios. *Chinese Sci. Bull.* 50, 2481–2486.
- Li, X.-H., Li, Z.-X., Sinclair, J.A., Li, W.-X., Carter, G., 2006. Revisiting the “Yanbian Terrane”: implications for Neoproterozoic tectonic evolution of the western Yangtze Block, South China. *Precambrian Res.* 151, 14–30.
- Li, X.-H., Li, Z.-X., Sinclair, J.A., Li, W.-X., Carter, G., 2007a. Reply to the comment by Zhou et al. on: “Revisiting the ‘Yanbian Terrane’: implications for Neoproterozoic tectonic evolution of the western Yangtze Block, South China” [*Precambrian Res.* 151 (2006) 14–30] [*Precambrian Res.* 154 (2007) 153–157]. *Precambrian Res.* 155, 318–323.
- Li, X.-H., Li, Z.-X., Sinclair, J.A., Li, W.-X., Carter, G., 2007b. Understanding dual geochemical characters in a geological context for the Gaojiacun intrusion: response to Munteanu and Yao’s discussion [*Precambrian Res.* 154 (2007) 164–167]. *Precambrian Res.* 155, 328–332.
- Liew, T.C., Hofmann, A.W., 1988. Precambrian crustal components, plutonic associations, plate environment of the Hercynian Fold Belt of central Europe: indications from a Nd and Sr isotopic study. *Contrib. Mineral. Petrol.* 98, 129–138.
- Lin, G.C., Li, X.H., Li, W.X., 2007. SHRIMP U–Pb zircon age, geochemistry and Nd–Hf isotope of Neoproterozoic mafic dyke swarms in western Sichuan: petrogenesis and tectonic significance. *Sci. China (D)* 50, 1–16.
- Ling, W.L., Gao, S., Zhang, B.R., Li, H.M., Liu, Y., Cheng, J.P., 2003. Neoproterozoic tectonic evolution of the northwestern Yangtze craton, South China: implications for amalgamation and break-up of the Rodinia Supercontinent. *Precambrian Res.* 122, 111–140.
- Ling, W.L., Gao, S., Cheng, J.P., Jiang, L.S., Yuan, H.L., Hu, Z.C., 2006. Neoproterozoic magmatic events within the Yangtze continental interior and along its northern margin and their tectonic implication: constraint from the ELA-ICPMS U–Pb geochronology of zircons from the Huangling and Hannan complexes. *Acta Petrol. Sinica* 22, 387–396.
- Liu, M., Shen, Y., 1998. Crustal collapse, mantle upwelling, and Cenozoic extension of the North American Cordillera. *Tectonics* 17, 311–321.
- Ludwig, K.R., 2001. Users Manual for Isoplot/Ex (rev. 2.49): A Geochronological Toolkit for Microsoft Excel, 1a. Berkeley Geochronology Center, Special Publication, 55 pp.
- Ma, G., Li, H., Zhang, Z., 1984. An investigation of the age limits of the Sinian System in South China. *Bull. Yichang Inst. Geol. Miner. Resour.* 8, 1–29 (in Chinese with English abstract).
- Ma, D., Du, S., Xiao, Z., 2002. The origin of Huangling granite batholith. *Acta Petrol. Mineral.* 21 (2), 151–161 (in Chinese with English abstract).
- Malavieille, J., Guihot, P., Costa, S., Lardeaux, J.M., Gardien, V., 1990. Collapse of the thickened Variscan crust in the French Massif Central: Mont Pilat extensional shear zone and St. Etienne Late Carboniferous Basin. *Tectonophysics* 177, 139–149.
- Martin, H., 1999. Adakitic magmas: modern analogues of Archean granitoids. *Lithos* 46, 411–429.
- Mayborn, K.R., Leshner, C.E., 2004. Paleoproterozoic mafic dike swarms of northeast Laurentia: products of plumes or ambient mantle? *Earth Planet. Sci. Lett.* 225, 305–317.
- McDonough, W.F., Sun, S.S., 1995. The composition of the earth. *Chem. Geol.* 120, 223–253.
- Munteanu, M., Yao, Y., 2007. The Gaojiacun intrusion: rift- or subduction-related?: comment on “Revisiting the ‘Yanbian Terrane’: implications for Neoproterozoic tectonic evolution of the western Yangtze Block, South China” by Li et al. (2006) [*Precambrian Res.* 151 (2006) 14–30]. *Precambrian Res.* 155, 324–327.
- Nebel, O., Nebel-Jacobsen, Y., Mezger, K., Berndt, J., 2007. Initial Hf isotope compositions in magmatic zircon from early Proterozoic rocks from the Gawler Craton, Australia: a test for zircon model ages. *Chem. Geol.* 241, 23–37.
- Nowell, G.M., Kempton, P.D., Noble, S.R., Fitton, J.G., Saunders, A.D., Mahoney, J.J., Taylor, R.N., 1998. High precision Hf isotope measurements of MORB and OIB by thermal ionisation mass spectrometry: insights into the depleted mantle. *Chem. Geol.* 149, 211–233.
- O’Neil, J.R., Chappell, B.W., 1977. Oxygen and hydrogen isotope relations in the Berridale batholith. *J. Geol. Soc. London* 133, 559–571.
- Patchett, P.J., White, W.M., Feldmann, H., Kielinczuk, S., Hofmann, A.W., 1984. Hafnium/rare earth element fractionation in the sedimentary system and crustal recycling into the Earth’s mantle. *Earth Planet. Sci. Lett.* 69, 365–378.
- Qiu, Y.M., Gao, S., McNaughton, N.J., Groves, D.J., Ling, W.L., 2000. First evidence of ≥ 3.2 Ga continental crust in the Yangtze craton of South China and its implications for Archean crustal evolution and Phanerozoic tectonics. *Geology* 28, 11–14.
- Ramsey, M.H., Potts, P.J., Webb, P.C., Watkins, P., Watson, J.S., Coles, B.J., 1995. An objective assessment of analytical method precision: comparison of ICP-AES and XRF for the analysis of silicate rocks. *Chem. Geol.* 124, 1–19.
- Rapp, R.P., Shimizu, N., Norman, M.D., 2003. Growth of early continental crust by partial melting of eclogite. *Nature* 425, 605–609.
- Rey, P., Vanderhaeghe, O., Teyssier, C., 2001. Gravitational collapse of the continental crust: definition, regimes and modes. *Tectonophysics* 342, 435–449.
- Rudnick, R.L., 1995. Making continental crust. *Nature* 378, 571–578.
- Scherer, E., Munker, C., Mezger, K., 2001. Calibration of the lutetium–hafnium clock. *Science* 293, 683–687.
- Smithies, R.H., 2000. The Archean tonalite–trondhjemite–granodiorite (TTG) series is not an analogue of Cenozoic adakite. *Earth Planet. Sci. Lett.* 182, 115–125.
- Sun, S.S., McDonough, W.F., 1989. Chemical and isotopic systematics of oceanic basalt: implications for mantle composition and processes. In: Sanders, A.D., Norry, M.J. (Eds.), *Magmatism in the Ocean Basins*, vol. 42. *Geol. Soc. Spec. Publ.*, pp. 313–345.
- Tang, J., Zheng, Y.-F., Wu, Y.-B., Gong, B., Zha, X.P., Liu, X.M., 2008. Zircon U–Pb age and geochemical constraints on the tectonic affinity of the Jiaodong terrane in the Sulu orogen, China. *Precambrian Res.* 161, 389–418.
- Taylor Jr., H.P., 1977. Water/rock interactions and the origin of H₂O in granitic batholiths. *J. Geol. Soc. London* 133, 509–558.
- Taylor, S.R., McLennan, S.M., 1995. The geochemical evolution of the continental crust. *Rev. Geophys.* 33, 241–165.
- Valley, J.W., 2003. Oxygen isotopes in zircon. *Rev. Mineral. Geochem.* 53, 343–385.
- Valley, J.W., Kitchen, N., Kohn, M.J., Niendorf, C.R., Spicuzza, M.J., 1995. UWG-2, a garnet standard for oxygen isotope ratios: strategies for high precision and accuracy with laser heating. *Geochim. Cosmochim. Acta* 59, 5223–5231.
- Vervoort, J.D., Patchett, P.J., Blichert-Toft, J., Albarede, F., 1999. Relationships between Lu–Hf and Sm–Nd isotopic systems in the global sedimentary system. *Earth Planet. Sci. Lett.* 168, 79–99.
- Wang, K., Plank, T., Walker, J.D., Smith, E.I., 2002. A mantle melting profile across the basin and range, SW USA. *J. Geophys. Res. (Solid Earth)*, 107 (B1), 2017. doi:10.1029/2001JB000209.
- Wang, X.L., Zhou, J.C., Qiu, J.S., Gao, J.F., 2004a. Comment on “Neoproterozoic granitoids in South China: crustal melting above a mantle plume at ca. 825 Ma?” by Xian-Hua Li et al. [*Precambrian Res.* 122 (2003) 45–83]. *Precambrian Res.* 132, 401–403.
- Wang, X.L., Zhou, J.C., Qiu, J.S., Gao, J.F., 2004b. Geochemistry of the Meso- to Neoproterozoic basic-acid rocks from Hunan Province, South China: implications for the evolution of the western Jiangnan orogen. *Precambrian Res.* 135, 79–103.
- Wang, X.L., Zhou, J.C., Qiu, J.S., Zhang, W.L., Liu, X.M., Zhang, G.L., 2006. LA-ICP-MS U–Pb zircon geochronology of the Neoproterozoic igneous rocks from Northern Guangxi, South China: implications for tectonic evolution. *Precambrian Res.* 145, 111–130.
- Williams, I.S., 1998. U–Th–Pb geochronology by ion microprobe. *Rev. Econ. Geol.* 7, 1–35.
- Wu, Y.-B., Zheng, Y.-F., Zhou, J.-B., 2004. Neoproterozoic granitoid in northwest Sulu and its bearing on the North China–South China Blocks boundary in east China. *Geophys. Res. Lett.* 31, L07616. doi:10.1029/2004GL019785.
- Wu, R.-X., Zheng, Y.-F., Wu, Y.-B., Zhao, Z.-F., Zhang, S.-B., Liu, X., Wu, F.-Y., 2006a. Reworking of juvenile crust: element and isotope evidence

- from Neoproterozoic granodiorite in South China. *Precambrian Res.* 146, 179–212.
- Wu, F.-Y., Yang, Y.-H., Xie, L.-W., Yang, J.-H., Xu, P., 2006b. Hf isotopic compositions of the standard zircons and baddeleyites used in U–Pb geochronology. *Chem. Geol.* 234, 105–126.
- Wu, Y.-B., Zheng, Y.-F., Tang, J., Gong, B., Zhao, Z.-F., Liu, X.M., 2007. Zircon U–Pb dating of water–rock interaction during Neoproterozoic rift magmatism in South China. *Chem. Geol.* 246, 65–86.
- Xie, Z., Zheng, Y.-F., Zhao, Z.-F., Wu, Y.-B., Wang, Z.R., Chen, J.F., Liu, X.M., Wu, F.-Y., 2006. Mineral isotope evidence for the contemporaneous process of Mesozoic granite emplacement and gneiss metamorphism in the Dabie orogen. *Chem. Geol.* 231, 214–235.
- Xu, P., Wu, F.Y., Xie, L.W., Yang, Y.H., 2004. Hf isotopic compositions of the standard zircons for U–Pb dating. *Chinese Sci. Bull.* 49, 1642–1648.
- Yuan, H.L., Gao, S., Liu, X.M., Li, H.M., Gunther, D., Wu, F.Y., 2004. Accurate U–Pb age and trace element determinations of zircon by laser ablation-inductively coupled plasma-mass spectrometry. *Geostand. Geoanal. Res.* 28, 353–370.
- Zhang, S.-B., Zheng, Y.-F., Wu, Y.-B., Zhao, Z.-F., Gao, S., Wu, F.-Y., 2006a. Zircon isotope evidence for ≥ 3.5 Ga continental crust in the Yangtze craton of China. *Precambrian Res.* 146, 16–34.
- Zhang, S.-B., Zheng, Y.-F., Wu, Y.-B., Zhao, Z.-F., Gao, S., Wu, F.-Y., 2006b. Zircon U–Pb age and Hf–O isotope evidence for Paleoproterozoic metamorphic event in South China. *Precambrian Res.* 151, 265–288.
- Zhang, S.-B., Zheng, Y.-F., Wu, Y.-B., Zhao, Z.-F., Gao, S., Wu, F.-Y., 2006c. Zircon U–Pb age and Hf isotope evidence for 3.8 Ga crustal remnant and episodic reworking of Archean crust in South China. *Earth Planet. Sci. Lett.* 252, 56–71.
- Zhao, J.-H., Zhou, M.-F., 2006. Geochemistry of Neoproterozoic mafic intrusions in the Panzhihua district (Sichuan Province, SW China): implications for subduction-related metasomatism in the upper mantle. *Precambrian Res.* 152, 27–47.
- Zhao, Z.-F., Zheng, Y.-F., Wei, C.-S., Gong, B., 2004. Temporal relationship between granite cooling and hydrothermal uranium mineralization at Dalongshan in China: a combined radiometric and oxygen isotopic study. *Ore Geol. Rev.* 25, 221–236.
- Zheng, Y.F., 1989. Influence of the nature of the initial Rb–Sr system on isochron validity. *Chem. Geol.* 80, 1–16.
- Zheng, Y.-F., 1993a. Calculation of oxygen isotope fractionation in anhydrous silicate minerals. *Geochim. Cosmochim. Acta* 57, 1079–1091.
- Zheng, Y.-F., 1993b. Calculation of oxygen isotope fractionation in hydroxyl-bearing silicates. *Earth Planet. Sci. Lett.* 120, 247–263.
- Zheng, Y.-F., 1995. Oxygen isotope fractionation in magnetites: structural effect and oxygen inheritance. *Chem. Geol.* 121, 309–316.
- Zheng, Y.F., Fu, B., 1998. Estimation of oxygen diffusivity from anion porosity in minerals. *Geochem. J.* 32, 71–89.
- Zheng, Y.F., Wang, Z.B., Li, S.G., Zhao, Z.F., 2002. Oxygen isotope equilibrium between eclogite minerals and its constraints on mineral Sm–Nd chronometer. *Geochim. Cosmochim. Acta* 66, 625–634.
- Zheng, Y.F., Wu, Y.B., Chen, F.K., Gong, B., Li, L., Zhao, Z.F., 2004. Zircon U–Pb and oxygen isotope evidence for a large-scale ^{18}O depletion event in igneous rocks during the Neoproterozoic. *Geochim. Cosmochim. Acta* 68, 4145–4165.
- Zheng, Y.-F., Zhao, Z.-F., Wu, Y.-B., Zhang, S.-B., Liu, X., Wu, F.-Y., 2006a. Zircon U–Pb age, Hf and O isotope constraints on protolith origin of ultrahigh-pressure eclogite and gneiss in the Dabie orogen. *Chem. Geol.* 231, 135–158.
- Zheng, J.-P., Griffin, W.L., O’Reilly, S.Y., Zhang, M., Pearson, N., Pan, Y., 2006b. Widespread Archean basement beneath the Yangtze craton. *Geology* 34, 417–420.
- Zheng, Y.-F., Zhang, S.-B., Zhao, Z.-F., Wu, Y.-B., Li, X.H., Li, Z.X., Wu, F.-Y., 2007. Contrasting zircon Hf and O isotopes in the two episodes of Neoproterozoic granitoids in South China: implications for growth and reworking of continental crust. *Lithos* 96, 127–150.
- Zhou, M.F., Kennedy, A.K., Sun, M., Malpas, J., Leshner, C.M., 2002a. Neoproterozoic arc-related mafic intrusions along the northern margin of South China: implications for the accretion of Rodinia. *J. Geol.* 110, 611–618.
- Zhou, M.F., Yan, D.P., Kennedy, A.K., Li, Y.Q., Ding, J., 2002b. SHRIMP U–Pb zircon geochronological and geochemical evidence for Neoproterozoic arc-magmatism along the western margin of the Yangtze Block, South China. *Earth Planet. Sci. Lett.* 196, 51–67.
- Zhou, J.C., Wang, X.L., Qiu, J.S., Gao, J.F., 2004. Geochemistry of Meso- and Neoproterozoic mafic-ultramafic rocks from northern Guangxi, China: arc or plume magmatism? *Geochem. J.* 38, 139–152.
- Zhou, M.F., Ma, Y.X., Yan, D.P., Xia, X.P., Zhao, J.H., Sun, M., 2006a. The Yanbian terrane (Southern Sichuan Province, SW China): a Neoproterozoic arc assemblage in the western margin of the Yangtze block. *Precambrian Res.* 144, 19–38.
- Zhou, M.-F., Yan, D.-P., Wang, C.-L., Qi, L., Kennedy, A., 2006b. Subduction-related origin of the 750 Ma Xuelongbao adakitic complex (Sichuan Province, China): implications for the tectonic setting of the giant Neoproterozoic magmatic event in South China. *Earth Planet. Sci. Lett.* 248, 286–300.
- Zhou, M.-F., Zhao, J.-H., Xia, X.P., Sun, W.-H., Yan, D.-P., 2007. Comment on “Revisiting the ‘Yanbian Terrane’: implications for Neoproterozoic tectonic evolution of the western Yangtze Block, South China” [*Precambrian Res.* 151 (2006) 14–30]. *Precambrian Res.* 155, 313–317.